Laboratory Assessment of Mercury Methylation in Response to Elevated Salinity in Everglades Peat

By

BRYCE COOK

THESIS

Submitted in partial satisfaction of the requirements for the degree of

MASTER OF SCIENCE

in

Agricultural and Environmental Chemistry

in the

OFFICE OF GRADUATE STUDIES

of the

UNIVERSITY OF CALIFORNIA

DAVIS

Approved:

Brett Poulin, Chair

Jasquelin Peña

Peter Hernes

Committee in Charge

2023

Abstract

Mercury (Hg) is a ubiquitous environmental contaminant that impacts aquatic environments and human health globally. Methylmercury (MeHg), the neurotoxic form of Hg that bioaccumulates and biomagnifies up aquatic food webs, is prominent in the Everglades' waters and organisms. Biogeochemical drivers controlling MeHg formation in the freshwater portion of the Florida Everglades include dissolved organic matter (DOM), which complexes inorganic divalent Hg (Hg(II)) and enhances lability for microbial methylation; sulfate (SO_4^{2-}) from agricultural inputs, which influence the presence and activity of organisms that impact Hg(II) methylation; and abundant inorganic Hg delivered to the Everglades by rainfall. The Everglades are particularly susceptible to conditions that increase SO_4^{2-} delivery and possibly Hg(II) methylation due to increasing magnitude, frequency, and duration of salinity spikes in Everglades National Park caused by sea level rise. In the Everglades, and globally, there is an urgent need to assess how Hg cycling will respond in coastal environments in light of rapidly rising sea level.

To investigate the effect of sea level rise on Hg(II) methylation, peat cores were collected from the freshwater Everglades and incubated in the lab for 0-20 days with water at 5 relevant salinity levels from 0.16 – 6.0 parts-per-thousand, representing SO_4^{2-} amendments from 0.2 to 450 mg L^{-1}, which represent a freshwater to brackish transition in coastal wetlands. Treatment waters were spiked with enriched stable 201Hg(II) isotope to track the transformation of ^{201}Hg(II) to Me^{201}Hg through time at each salinity treatment, accounting for speciation of native Hg in peat cores at time of core flooding. At 8 time points from 0-20 days, porewater was sampled from peat cores and analyzed for relevant geochemical constituents and the transformation of inorganic ^{201}Hg(II) to Me^{201}Hg. Peat was also measured for concentrations of inorganic ^{201}Hg(II) and Me^{201}Hg.

In all five salinity treatments, shortly after inundation, the porewater became anoxic and with increased incubation time the DOM composition shifted to more aromatic in composition, as evidenced by DOM $SUVA_{254}$ across all five salinities. In the four highest salinity treatments, SO_4^{2-} concentrations decreased and sulfide concentrations increased with incubation time due to microbial dissimilatory SO_4^{2-} reduction.

The shifts to microbial SO_4^{2-} reduction temporally aligned with observed conversion of $^{201}Hg(II)$ to $Me^{201}Hg$ at each of the elevated salinity. Although there were no statistical differences in total $Me^{201}Hg$ production between the five salinity treatments (porewaters plus peat), $Me^{201}Hg$ formed at elevated salinity was present at higher concentrations in the porewaters (as opposed to associated with the peat). This result is interpreted to be due to porewater MeHg stabilization by aqueous complexation of MeHg by ligands such as aromatic DOM and sulfide at higher salinity treatments, inhibiting binding of MeHg to the peat sediment substrate. Overall, the experiments demonstrate that salinity intrusion can result in pronounced MeHg production in porewaters. The produced MeHg is expected to be highly mobile for coastal export to coastal marine ecosystems due to via rising and falling tidal cycles which flush estuarine peat regularly, having implications for MeHg uptake in coastal aquatic food webs.

Acknowledgements

This research was conducted with support from the Poulin Lab at the University of California – Davis, Davis CA and the USGS Mercury Research Laboratory, Madison WI. I would like to thank undergraduate students Tiffany Tat, Tracy Tran, and Jeff Murray for providing analytical support, as well as Dr. Tran Nguyen's lab at the University of California – Davis for providing reagents for synthetic water. This research was funded by the U.S. Geological Survey Greater Everglades Priority Ecosystems Science (GEPES) Program and the Everglades Foundation and Volo Foundation through the Foreverglades graduate research fellowship.

Table of Contents

Introduction

Mercury (Hg) is a ubiquitous environmental neurotoxin that impacts all aquatic environments and humans globally, with humans typically exhibiting total Hg blood concentrations from 0.5-2 ug/L depending on dietary exposure to Hg.[1] In aquatic environments, Hg can be transformed by microorganisms to toxic methylmercury[2] (MeHg) which bioaccumulates in food webs to toxic levels in fishes and other aquatic organisms.[3] In the Florida Everglades, MeHg accumulates in predator fishes like largemouth bass (1.31 mg/Kg mean total Hg), wading birds such as herons (21.3 mg/Kg mean total Hg) and egrets (19.8 mg/Kg mean total Hg), the American alligator (2.18 mg/Kg mean total Hg), and the Florida panther (55.5 mg/Kg mean total Hg in hairs), and in some instances has shown to alter organism behavior.[4] Humans also face risk of Hg poisoning from consumption of fish and apex predators. The risk of Hg toxicity is highest among women and communities with high fish diets (e.g., those reliant on subsistence fishing), and is especially a concern to children and infants whose nervous systems are still developing.[1] In freshwater and coastal environments, local biogeochemical processes control the environmental exposure of wildlife and humans to Hg by mediating the production, fate, and transport MeHg. In the Florida Everglades, mangrove forests populate coastal terrestrial to marine transition zones and have previously been identified as drivers of MeHg export to coastal waters.[5] Coastal ecosystems are well poised for formation, export, and biological accumulation of toxic MeHg due to their unique positioning between marine and terrestrial systems, both of which are susceptible to natural and anthropogenic perturbations such as sea level rise, which may exacerbate the issue of MeHg contamination.

Sea level rise, a result of melting polar ice caps and the thermal expansion of the ocean, are threatening coastlines globally.[6] The southern Florida Everglades are a particularly at-risk region for sea level rise as approximately one-third of the greater Everglades are within 1.5 m of sea level, and half of the Everglades National Park lies below 0.6 m of sea level.[7] Further, the southern Florida Everglades have a very gradual elevation slope of about 5 cm per mile, increasing the risk of large-scale inundation.[5] By 2060, sea levels in South Florida are conservatively expected to rise 0.60 m which will cause increases in salinity and

inundation in both brackish and freshwater areas of the southern Florida coast,[7] though this may be partially combatted with increased freshwater delivery from restoration efforts. In the Everglades, and globally, there is an urgent need to assess how Hg cycling will respond in coastal environments in light of rapidly rising sea level.

Sea level rise could have multi-dimensional effects on the biogeochemical processes that control the formation of MeHg in aquatic environments. Broadly, MeHg formation is governed by the synergy between (1) the potential of the microbial community to methylate inorganic divalent Hg (Hg(II)), based on abundance of the pre-requisite *hgcAB* genes, and (2) the bioavailability of Hg(II).[8] Both of these processes are influenced by Sulfate (SO_4^{2-}) concentrations, a key environmental constituent which impacts the geochemical and microbial processes governing Hg methylation in diverse wetlands and estuaries[9–12] including freshwater portions of the Florida Everglades.[12–14] SO_4^{2-} is understood to stimulate SO_4^{2-} reducing bacteria (SRB), which utilize SO_4^{2-} as a terminal electron acceptor in dissimilatory SO_4^{2-} reduction, fueling anaerobic respiration. SRB in the freshwater Florida Everglades, while found to contain low abundance of the Hg(II) methylation gene pair[8] *hgcAB*, are further proposed stimulate overall microbial metabolism linked to MeHg production through consumption of fermentative products[15] and/or by stimulating methanogenic activity through syntrophy.[12,16] Dissimilatory SO_4^{2-} also serve to increase the release and production of high molecular weight and aromatic dissolved organic matter (DOM) from peat that promotes Hg(II) bioavailability.[17,18] DOM promotes Hg(II) bioavailability through complexation with DOM thiol moieties[19] and capping the formation of larger nanocolloidal metacinnabar (nano-β-$HgS_{(s)}$) aggregates under mildly sulfidic conditions, keeping Hg(II) poorly crystalline, suspended in solution, and available to microbial communities for methylation.[2,17,20,21] SO_4^{2-} reduction also results in enrichment of DOM reduced sulfur content that bind Hg(II) and MeHg[22] and the increases DOM $SUVA_{254}$ (a spectral proxy for aromaticity).[23] Further, MeHg enters the food web through accumulation of MeHg in periphyton and phytoplankton in the water column;[24–27] thus the partitioning of Hg(II) and MeHg from peat sediments to surrounding porewaters – and to the water column and coastal ecosystems through diffusion and tidal

pumping[5] – is likely to be a key driver of MeHg bioaccumulation in coastal systems. While these biogeochemical controls are well documented and understood in the freshwater Everglades, impending global climate change is likely to have a significant impact on the aquatic biogeochemistry of coastal wetlands due to rising sea levels. Specifically, seawater has a significantly higher SO_4^{2-} concentration compared to the freshwater Florida Everglades.

Here, we present results of the first laboratory evaluation of the biogeochemical response of Hg(II) methylation to salinity intrusion using peat cores collected from freshwater Florida Everglades. Intact peat cores were saturated with water at five salinity levels (0.16 ppt – 6.0 ppt) that included an enriched stable isotope of Hg(II) to quantify methylation and partitioning of Hg(II) and MeHg from porewaters to peat over 20 days of saturation. Over the 20 day incubation, cores were vertically profiled for redox state and porewater was sampled and analyzed for key biogeochemical constituents pertinent to Hg (i.e., SO_4^{2-} and sulfide, DOM concentration and composition). We discuss the experimental results in context of the impacts of sea level rise on MeHg formation, partitioning, and potential export to coastal ecosystems.

Methods

Site Description and Core Collection

Replicate peat cores (n = 125) were collected from a historically low SO_4^{2-} site[28] (1.2 ppm SO_4^{2-} in the porewater at time of core collection) in Water Conservation Area 3A (WCA-3A, Subsite H) of the Florida Everglades (**Figure 1**). This site was selected for peat core collection because (1) it has historically experienced minimal impact[28] by agricultural SO_4^{2-} and is not influenced by marine SO_4^{2-}, and (2) it mimics sawgrass-dominated Everglades wetlands in the intertidal region of Shark River Slough that is currently experiencing sea level rise. Concurrent with peat core collection, porewater and surface water were sampled for measurement of DOC concentration, DOM composition by optical measurements, inorganic anions, filter-passing total Hg, and filter-passing MeHg. Other relevant field chemical characteristics of the site surface and porewater were recorded on site, including pH, conductivity, oxidation-reduction potential

(ORP), dissolved oxygen (DO), total inorganic dissolved sulfide (S^{2-}), and temperature (**Table 1**). Cores were collected within a 20-meter radius area by gently inserting 15.2 cm tall polycarbonate tubes (7.62 cm outside diameter) directly into submerged peat. Peat cores were flooded with site water, capped with no headspace, and shipped on wet ice to the University of California, Davis for experimentation. Cores were stored at 4˚ C in the dark for 72-219 days until use in incubation experiments.

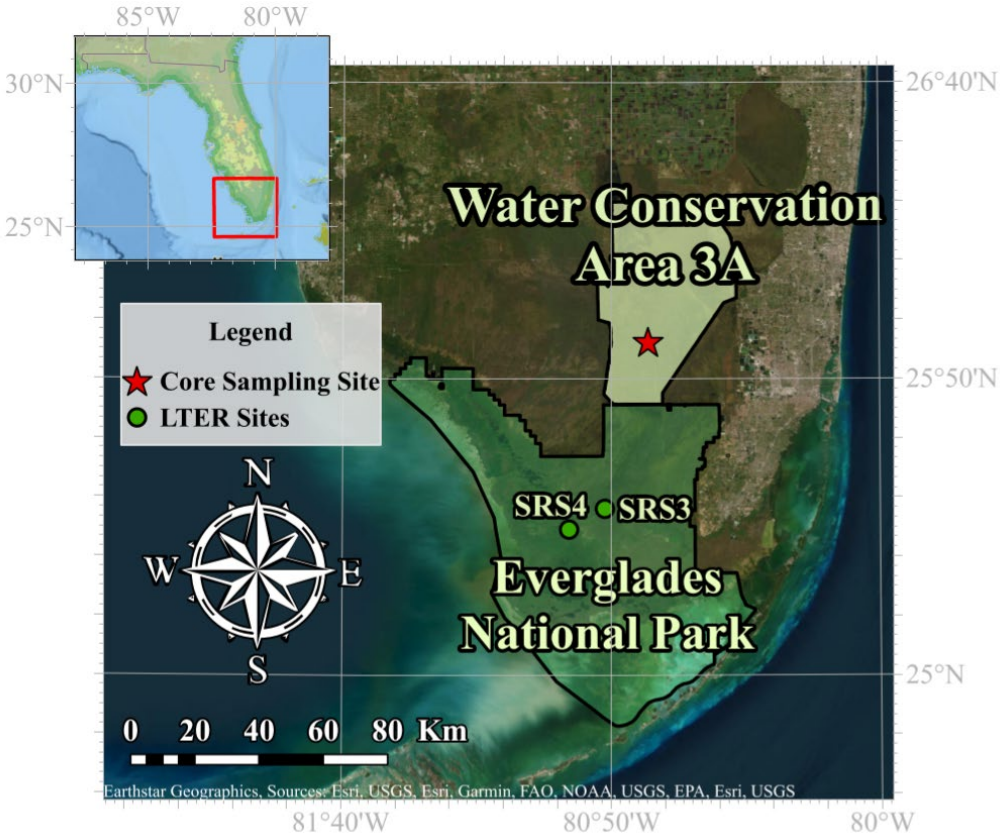

Figure 1. Map of location that peat cores were collected in Water Conservation Area 3A (subsite H) and LTER sites (SRS-3, SRS-4) within Shark River Slough of Everglades National Park.

Table 1. Ancillary conditions and chemical measurements at Water Conservation Area 3A, Subsite H at the time of peat core collection

Parameter	*Surface Water*	*Porewater*
DOC (mg C L^{-1})	15.0	22.2
DOM $SUVA_{254}$ (L mg C^{-1} m^{-1})	3.73	3.95
SO_4^{2-} (mg L^{-1})	0.7	1.2
Cl^- (mg L^{-1})	22.2	36.4
S^{2-} (mg L^{-1})	--	0.17
Filter-passing THg (ng L^{-1})	1.02	0.39
Filter-passing MeHg (ng L^{-1})	0.044	0.018
pH	6.96	6.34
ORP (mV)	--	-318.6
Conductivity (µS cm^{-1})	288.9	505.4
Dissolved Oxygen (% saturation)	56.2	0.12
Temperature (˚C)	30.9	29.1
Turbidity (FNU)	1.51	---

Laboratory Core Flooding Experiments: Porewater Chemistry

Laboratory experiments were carried out to quantify the biogeochemical responses of salt-water intrusion on Hg(II) methylation in intact Everglades peat. Core flooding experiments were carried out at five salinities (0.16 parts-per-thousand (ppt), 0.25 ppt, 0.50 ppt, 1.0 ppt, 6.0 ppt); this salinity regime was selected based on several observations. First, changes in the biogeochemical cycling of carbon and SO_4^{2-} have been observed in peat soil incubations with amended salinity ranging from 3-5 ppt.[29–31] Second, a decadal analysis of SO_4^{2-} and MeHg trends in Everglades National Park identified intertidal marsh and coastal mangrove sites with consistently elevated levels of SO_4^{2-} (Avg_{11year} = 5.50 ± 5.59 mg L^{-1}) with anomalously high levels of MeHg (Avg_{11year} = 0.19 ± 0.15 ng L^{-1}) compared to the freshwater marsh sites.[23] Third, we conducted a temporal analysis of salinity data measured at two sites in Shark River Slough (Dec 2000 – Dec 2021; sites SRS-4 and SRS-3), shown in **Figure 2**, which compares salinity regimes of wetlands that exhibit tidally and seasonally fluctuations in salinity.[32] At site SRS-4 (shown in **Figure 1**), the site with a higher salinity regime, seasonal variation in surface water salinity (0.1 – 24.4 ppt) is driven by changes in the freshwater hydraulic head during the rainy season (May - October) compared to the dry season

(November - April) (**Figure 2A**). At SRS-3 (shown in **Figure 1**), which is 12.9 km inland from SRS-4, the salinity was consistently freshwater in character (0.1-1.4 ppt) (**Figure 2B**). With rising sea levels expected throughout the 21st century,[33] peat previously unimpacted by seawater intrusion, at site SRS-3 for instance, will begin to experience gradual increases in salinity, as observed in porewaters[34] at site SRS-4 (**Figure 2C**). Thus, peat core flooding experiments of this study evaluated the initial responses to modest increases in salinity observed at the onset of saltwater intrusion of peat wetlands (≤ 6 ppt).

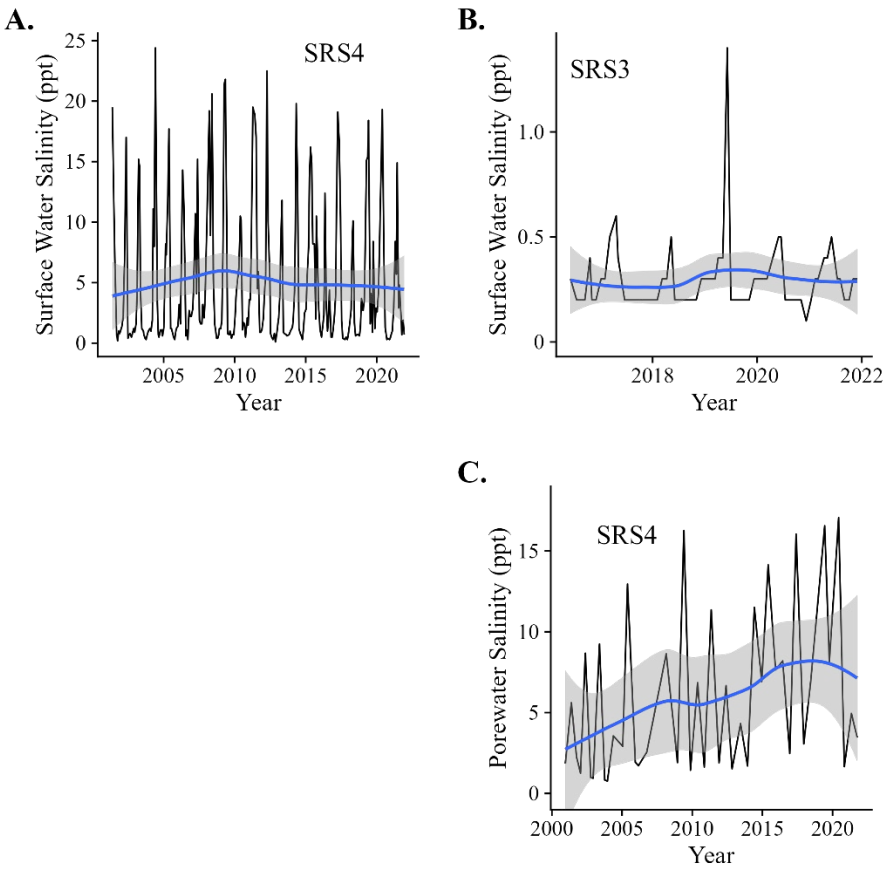

Figure 2. Salinity (parts-per-thousand, ppt) measurements at Shark River Slough LTER sites including (a) surface water at SRS3, (b) surface water at SRS4, and (c) porewater at SRS4. In each plot, the black line, blue line, and gray shaded area present the measured salinity, locally smoothed LOESS regression, and associated 95% confidence interval, respectively.

In the laboratory, peat cores were flooded (**Figure 3**) with water of uniform DOM chemistry (5.5 mg C L^{-1}) and near uniform pH, with salinity being the only major difference between treatment waters. First,

a 12 ppt seawater stock solution was prepared with high purity water (>18.2 MΩ cm) and "Sea-Salt" ASTM D 1141-98, Formula A (Lake Products Company LLC, Florissant, MO). Separately, the 0.16 ppt salinity endmember was prepared from salts to mimic the ionic composition of the freshwater Everglades wetlands (**Table 2**).[28] These two salinity endmembers, 0.16 and 12 ppt, were mixed at specific ratios to prepare the salinity waters of 0.25, 0.50, 1.0, and 6.0 ppt (**Table 3**). Next, a DOM stock solution was prepared with 75% Everglades F1 hydrophobic organic acids fraction (HPOA) and 25% Everglades F1 transphilic organic acid fraction (TPIA) previously isolated on XAD resins[35] from the Florida Everglades F1 site and characterized for DOM sulfur speciation.[22] This DOM was used because it mimics, generally, the nature of DOM in the Everglades and is absent of inorganic impurities.[22,35] The DOM stock solution was adjusted to pH 7 with 0.1 M NaOH and measured for DOC concentration on a Shimadzu TOC-L equipped with an NDIR detector. Across all salinity treatments, isotopically enriched ^{201}Hg(II) was added to treatment water to track Hg(II) methylation. To prepare the enriched ^{201}Hg(II) isotope spike for the peat cores used for the core flooding experiments, enriched ^{201}Hg(II) was added to the concentrated DOM stock solution in a 125 mL amber bottle and diluted to final ^{201}Hg(II) and DOC concentrations of 202 μg L^{-1} ^{201}Hg(II) and 552 mg C L^{-1}, respectively. It is estimated that the Hg(II) concentration was < 25% of the total strong thiol binding sites of F1 HPOA, based on a previous binding study of this DOM.[19] The DOM-^{201}Hg(II) solution was equilibrated for 24 hours prior to use in peat incubation experiments to ensure the added Hg(II) tracer equilibrated with the DOM ligands in the porewater. The ^{201}Hg(II)-DOM spike was added to separate 10 L carboys, also containing the five treatment salinities, to a final concentration of 1,480 ng L^{-1} ^{201}Hg(II) and 5.5 mg L^{-1} DOC (**Table 4**). The concentration of ^{201}Hg(II) isotope added was chosen to approximately double the ambient ^{201}Hg(II) signal from the peat[28] presuming that a large fraction of added isotope from the treatment water would bind strongly to the organic rich peat substrate in the core incubation experiment. DOC concentrations were chosen to approximate DOC concentrations in pristine marsh sites within Everglades National Park (Avg_{11year} = 11.0 ± 3.3 mg L^{-1})[23] and to ensure that the amended Hg(II) was provided in a bioavailable form.[8,17] The compositions of the five salinity treatment waters are presented in **Table 4**. The five waters at the target salinities were then immediately used to fill peat cores.

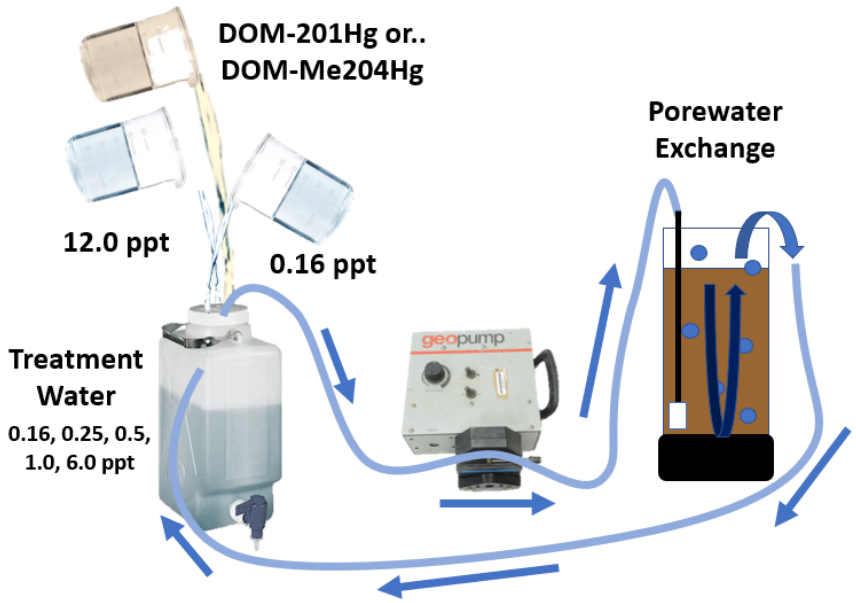

Figure 3. Schematic diagram demonstrating peat core flooding and porewater exchange with treatment water.

Table 2. Mass of salts dissolved in 20 L of high purity (>18.2 MΩ cm) water for the 0.16 ppt treatment water

Synthetic Everglades Freshwater Recipe (0.16 parts-per-thousand)		
Salt	**Mass (g)**	**Supplier**
$CaCl_2$	0.6662	Sigma-Aldrich
Na_2SO_4	0.0057	Sigma-Aldrich
$NaHCO_3$	0.7497	Sigma-Aldrich
$CaCO_3$	0.8990	Mallinckrodt
$MgCl_2 \cdot 6H_2O$	0.7115	Sigma-Aldrich

Table 3. Endmember mixing scheme used for the five treatment water salinity levels used in the peat core incubation

Treatment water mixing scheme		
Salinity	**Vol. of 0.16 ppt (L)**	**Vol. of 12 ppt (L)**
0.16 ppt	15.00	0
0.25 ppt	14.89	0.11
0.50 ppt	14.62	0.38
1.0 ppt	13.94	1.06
6.0 ppt	7.61	7.39

Table 4. Overview of chemical composition for each treatment salinity

Components from Synthetic Sea Water					
Salinity (ppt)	**0.16**	**0.25**	**0.50**	**1.0**	**6.0**
Cl^- (mg L^{-1})	31.9	248	409	505	3,340
Na^+ (mg L^{-1})	10.3	37.9	114	268	1800
SO_4^{2-} (mg L^{-1})	0.3	33.0	60.8	93.7	499
Mg^{2+} (mg L^{-1})	4.21	7.51	16.7	35.0	218
Ca^{2+} (mg L^{-1})	29.7	30.6	32.8	37.4	83.2
K^+ (mg L^{-1})	--	0.997	3.77	9.31	64.7
HCO_3^- (mg L^{-1})	80.4	80.2	79.5	78.1	64.5
Br^- (mg L^{-1})	--	0.170	0.642	1.59	11.0
$B(OH)_3$ (mg L^{-1})	--	0.0677	0.256	0.632	4.39
Sr^{2+} (mg L^{-1})	--	0.0347	0.131	0.323	2.25
F^- (mg L^{-1})	--	3.40E-03	0.0129	0.0318	0.221
Components from Everglades DOM stock solution					
DOC (mg L^{-1})	5.5	5.5	5.5	5.5	5.5
^{201}Hg(II) (ng L^{-1})	1,481	1,481	1,481	1,481	1,481

Laboratory Core Flooding Experiments: Incubations

The following steps were carried out for each of the five salinity treatments. Prior to flooding the cores with the salinity water, 21 cores were drained of site water by decanting excess water and equilibrated to 25 ± 2 ˚C . Core were carefully flooded with treatment water to ensure sufficient equilibration between peat and the treatment water. A borosilicate glass dispersion sparger was carefully inserted through the peat to the bottom of a core (without disturbing the peat integrity) and incubation water was slowly introduced with a peristaltic pump (Geotech) (**Figure 4**). Incubation water was pumped into the core and allowed to overflow the top of the core until the conductivity in the center of the core, as measured by an *in-situ* conductivity electrode (Amber Science, Model 2052), equaled the conductivity of the treatment water, (approximately 1-2 L of flow-through). On average, approximately 2 cm of standing water was overlying the peat sediment-water interface at the start of the experiment. For Hg(II) methylation experiments, 16 cores were flooded with treatment water amended with the inorganic ^{201}Hg(II) spike. Once filled, the cores

were covered with parafilm with puncture holes to allow for gas exchange, wrapped in foil, and stored on a laboratory bench at room temperature (25 ± 2 ˚C).

Figure 4. Photo of the process used to fill peat cores. A Geotech pump (middle) delivered the incubation water from the reservoir (right) to the bottom of the core (left). Water was allowed to flow up and out of the core. A conductivity electrode confirmed when the conductivity within the core was equal to the incubation water

For Hg(II) methylation experiments, duplicates cores were incubated for 0, 1, 2, 3, 6, 10, 13, 15, and 20 days to quantify the impacts of salinity on methylation for up to 20 days. Cores were sacrificed when sampled. Complete details on the sampling procedure are provided in **Figure 5**. For each treatment and time point (except for the 0.5 ppt treatment due to electrode malfunction), one of the duplicate cores at each time point was vertically profiled from the surface of the water to a depth of 6 cm (250 µm intervals; Unisense Field Microsensor Multimeter) for dissolved $O_{2\ (g)}$, hydrogen sulfide gas ($H_2S_{(g)}$), Oxidation-Reduction Potential (ORP), $H_{2\ (g)}$, and pH (**Figure 6**); microsensors were calibrated weekly. Temperature was recorded in the center of the profiled core with a thermocouple (AZ Instrument 4 channel K thermocouple). After the core was profiled, the porewater was sampled from replicate cores separately and filtered with Geotech inline 0.45 µm high-capacity non-woven acrylic copolymer filters. A subsample of

filtrate was preserved with Sulfide-Antioxidant Buffer (SAOB; ThermoScientific) within 1 minute of filtration for total sulfide (S^{2-}) determination via an Accumet Sulfide Ion-Selective Electrode (ISE). pH was determined on an unpreserved subsample of filtrate within 1 minute of filtration with a ThermoScientific Ross Ultra pH/ATC Triode. The remaining porewater sample was diluted 2-fold with high purity water (>18.2 MΩ cm) and then subsampled for the analyses detailed directly below. Peat from each core incubation were weighed for total wet mass and homogenized. Subsamples were collected from the homogenized peat, weighed, and frozen at -80˚C in 50 mL falcon centrifuge tubes for Hg analyses.

Figure 6. Photo of peat core being microprofiled with microelectrodes. Electrodes profile vertically 6 cm downwards from the water surface at a measurement interval of 250 µm.

Laboratory Core Flooding Experiments: Water and Peat Analyses

A subsample of the diluted porewater filtrate was preserved at 4˚C in a 125 mL amber bottle (pre-baked at 450˚C for 4 h) for DOC quantification by a Shimadzu TOC-L carbon analyzer, DOM UV-vis and fluorescence optical analyses via a Horiba Aqualog spectrofluorometer, conductivity quantification via an Orion conductivity cell, and total iron quantification via Hach 2700 Spectrophotometer utilizing EPA method 8008. Excitation-emission matrices (EEMs) (ex: 200-850 nm, em: 250-830 nm, resolution: 2 nm, integration time: 2 sec) and DOM absorbance spectra (resolution: 2 nm) were processed in R using the staRdom package[36] to provide decadic absorption coefficient at 254 nm (α_{254}) and spectral slope ratio (S_R)[37]. The specific UV absorbance at 254 nm ($SUVA_{254}$)[38] was calculated by dividing $\alpha_{254}(m^{-1})$ by the DOC concentration (mg C L^{-1}). Each of these parameters is further defined in **Table 5**. Porewater samples for inorganic anions (SO_4^{2-}, Cl^-, NO_3^-) determination were frozen in acid-cleaned, 30 mL low-density polyethylene bottles, and thawed for quantification on a Metrohm 881 Compact IC pro (Metrosep A supp 5 guard column, Metrosep A supp 7 main column). Mercury measurements were taken at all time points except at day 13. Mercury samples were acidified to 1% hydrochloric acid (HCl; OmniTrace) in sterile 500 mL polyethylene terephthalate glycol bottles and stored at room temperature. Total filter-passing Hg (THg) was quantified on a Brooks Rand MERX-T system following EPA method 1631e. Filter-passing aqueous excess total ^{201}Hg was determined by BrCl oxidation, $SnCl_2$ reduction, purge and trap, and detected and quantified via inductively coupled argon plasma mass spectrometry (Brooks Rand Merx-T; Thermo-Fisher iCAP-RQ ICP-MS). Total filter-passing Hg measurements were validated with bracketed QC standards and sample matrix spikes with ±20% recovery criteria. Total filter-passing $Me^{201}Hg$ isotope was quantified by isotope dilution, distillation, aqueous ethylation, purge and trap, and gas chromatography facilitated by a Brooks Rand MERX-M system and detected and quantified via Thermo-Fisher iCAP-RQ ICP-MS. Filter-passing MeHg measurements were validated by bracketed QC standards and sample matrix spikes with ±25% recovery.

Table 5. Absorbance indices measured on incubation core porewaters

Absorbance Indices			
Index	Calculation	Purpose	Reference
$SUVA_{254}$ - Specific ultra-violet absorbance at 254 nm	Absorption coefficient at 254 nm divided by DOC concentration	Higher number associated with greater aromatic content	[38]
S_R Spectral Slope Ratio	Spectral slope $S_{275-295}$ divided by spectral slope $S_{350-400}$	Negatively correlated to DOM molecular weight	[37]

Peat samples were freeze dried with a Labconco FreeZone freeze drier at -40˚C under 0.069 mm Hg pressure for a minimum of 3 days. Freeze dried peat samples were then weighed for dry mass and homogenized via a MP bead beater for 10 seconds at 4.0 m s^{-1}. Freeze dried peat samples for total Hg isotope analysis were weighed in digestion vessels and microwave digested following EPA method 3051a in 5 mL concentration HNO_3 (OmniTrace), ensuring that sediments reached 175±5˚C for 10 min. Digest samples were brought up to 50 mL total volume with high purity water (>18.2 MΩ cm), filtered with glass-fiber filters (Pall Corporation Acrodisc 25mm, 1μm glass fiber), brominated at 1% BrCl for at least a week, and quantified for Hg isotopes on a Brooks Rand MERX-T system by $SnCl_2$ reduction, purge and trap, and detected and quantified by cold vapor atomic fluorescence (CVAFS) spectroscopy and Thermo-Fisher iCAP-RQ ICP-MS. Total sediment Hg measurements were validated with bracketed QC standards and sample duplicates with ±20% recovery. Ambient and isotopically enriched MeHg species were quantified on sediments by isotope dilution, distillation, aqueous ethylation, purge and trap, and gas chromatography facilitated by a Brooks Rand MERX-M system and detected and quantified via Thermo-Fisher iCAP-RQ ICP-MS. Sediment MeHg measurements were validated by bracketed QC standards and sample matrix spikes with ±25% recovery.

Laboratory Core Flooding Experiments: Modelling

Modelling for redox-active Fe species in experimental core porewaters was performed using MINEQL$^+$ 5.0.[39] To model controls on Fe(II) solubility, an ionic strength titration was performed from the ionic strength of the 0.16 ppt treatment group up to 6.0 ppt. Modelling conditions (**Table A-1**) were chosen to mimic the porewater conditions of sulfide concentration, pH, and redox conditions of experimental cores at day 20. Solid phases were considered with the exception of pyrite, the formation of which is not a thermodynamically favorable process compared to other Fe sulfide ($FeS_{(s)}$) mineral species.

Results and Discussion

Porewater Chemistry of Peat Incubations

For each of the five treatment salinities (0.16, 0.25, 0.5, 1.0, and 6.0 ppt), porewater pH fluctuated between 6 and 7 from day 0 to day 20 (**Figure 7A**) with no statistical difference between time at each salinity ($p > 0.05$, one-way ANOVA, $n = 105$) and an observed statistical effect of salinity on pH with higher salinity treatments exhibiting modestly lower pH values ($p < 0.05$, one-way ANOVA, $n=105$). The observed circumneutral pH values correspond with other literature values from Everglades peat core salinity intrusion incubations of 6.8 at 3.5 ppt seawater[30], as well as with measured surface water pH values from the freshwater Florida Everglades[28]. Conductivity and chloride (Cl^-) measurements (**Figure 7B** and **7C**) of porewater at each salinity through time confirmed that cores from each of the five treatment salinities received a treatment water with statistically unique ionic composition (Bonferroni corrected pairwise t-test, $p<0.001$).

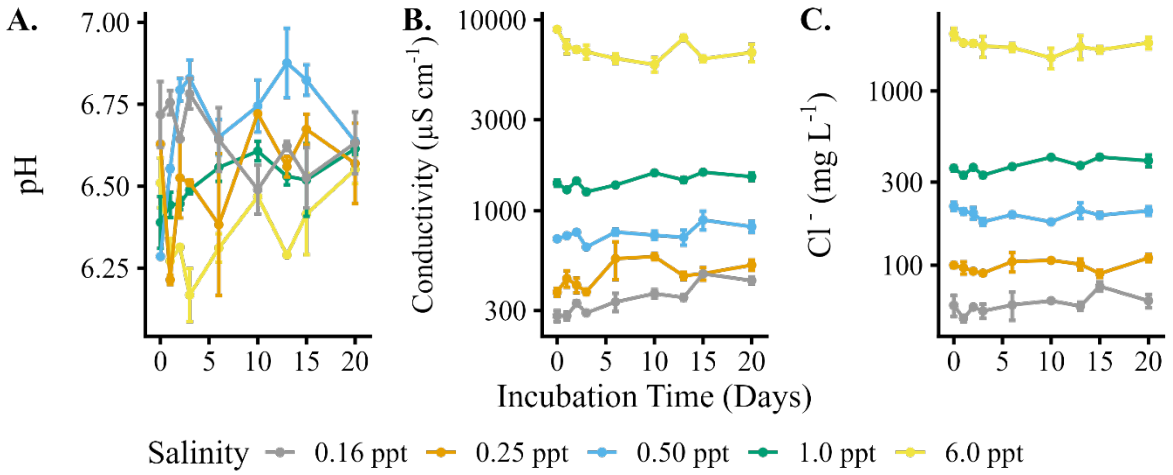

Figure 7. Porewater (A) pH, (B) conductivity (µS cm^{-1}), and (C) chloride (Cl^-, mg L^{-1}) at each of the five salinities as a function of incubation time (days). Data points present average values of experimental duplicates and error bars present standard error of the mean.

The chemistry of porewaters from peat incubations exhibited consistent trends of more reducing conditions with increased incubation time and notable differences in redox conditions between the five salinities. Peat cores were incubated with water saturated with dissolved $O_{2(g)}$, and all incubation porewaters were completely anoxic by day 1 ($O_{2(g)} \leq 0$ µmol L^{-1}). Porewater oxidation-reduction potential values (ORP), measured at 6 cm depth in the cores using the redox-profiler, were initially between 302 ± 44 – 475 mV at day 0 and decreased with increased incubation time (**Figure 8A**). Between days 10-20, the two highest salinity treatments (1.0 and 6.0 ppt) demonstrated statistically lower ORP values (-54.4 ± 15.4 mV and 0.00 ± 28.6 mV by day 20, respectively) compared to the other three salinity treatments (0.16, 0.25, 0.5 ppt) (Tukey, $p<0.05$, $n = 40$).

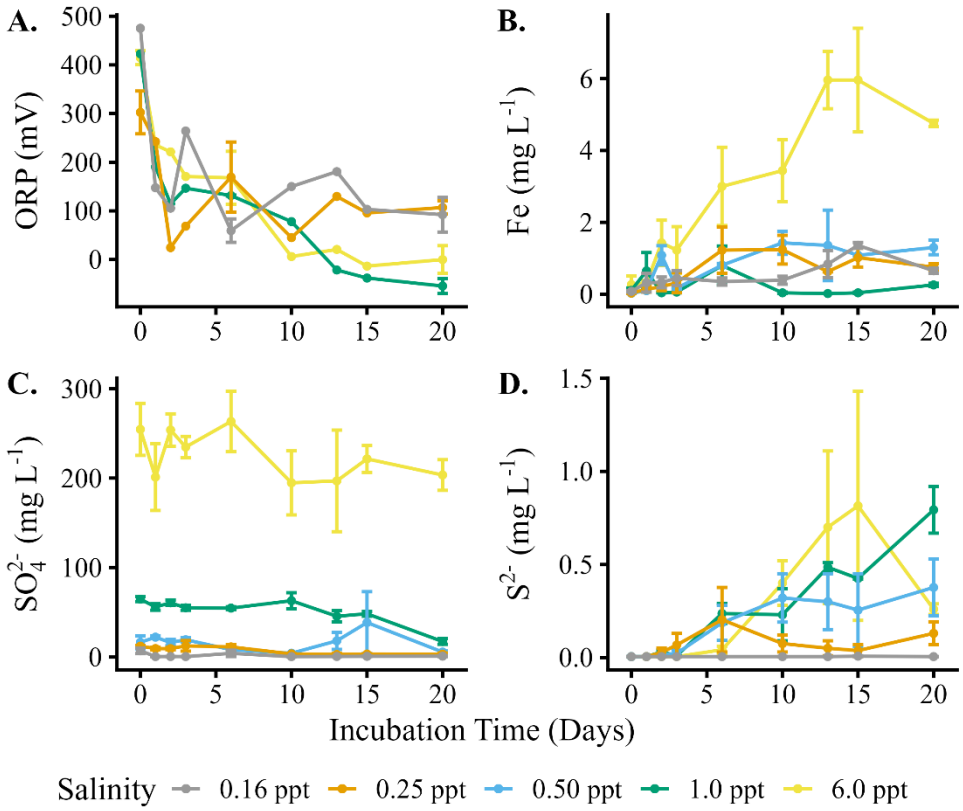

Figure 8. Porewater (A) oxidation-reduction potential (ORP) values at 6 cm depth from water surface compared to standard hydrogen electrode and porewater concentrations of (B) filter-passing total iron (Fe), (C) sulfate (SO_4^{2-}), and (D) total sulfide (S^{2-}). Data points present average values of experimental duplicates and error bars represent the standard error of the mean.

Total iron (Fe) was below detection in the treatment waters but was dynamic in incubation porewaters through time (**Figure 8B**). At day 0, filter-passing total Fe concentrations were less than 0.1 mg L^{-1} in porewaters of 0.16, 0.25, and 0.5 ppt treatments and less than 0.3 mg L^{-1} in the 1.0 and 6.0 ppt treatments. In the 6 ppt treatment, there was a pronounced increase in filter-passing total Fe concentration (e.g., 5.96 mg L^{-1} by day 13) that was significantly higher than the other salinity treatments ($p < 0.05$, Tukey, $n = 105$). By day 20, the 6 ppt treatment demonstrates the highest levels of porewater total Fe (4.8±0.1 mg L^{-1}) and the 1.0 ppt treatment demonstrates the lowest Fe concentration (0.26 ±0.05 mg L^{-1}), while the other treatments exhibited comparable and intermediate total Fe concentrations between the 6.0 and 1.0 ppt treatments.

SO_4^{2-} concentrations of the incubation waters, which varied at the start of incubations (**Table 4**), established the hierarchy in SO_4^{2-} levels at t = 0 days, which spanned from 7.0±3.1 to 254±29 mg L^{-1} in 0.16 and 6 ppt salinity treatments, respectively. In general, SO_4^{2-} concentrations decreased with increased incubation time (**Figure 8C**). In the four treatments of 0.16-1.0 ppt salinity, 66-87% of initial SO_4^{2-} was depleted by day 20, whereas only 20% of initial SO_4^{2-} is depleted in the 6.0 ppt treatment by day 20 (**Figure 8C**). Total sulfide (summation of $H_2S_{(aq)}$ and HS^-) concentrations from both the 1.0 and 6.0 ppt treatment groups statistically differ from the freshwater 0.16 ppt treatment ($p < 0.02$, Dunnett, n = 105) with higher total sulfide concentrations (0.79 ± 0.13 mg L^{-1} and 0.26 ± 0.03 mg L^{-1}) by day 20 than the freshwater 0.16 ppt treatment (< detection limit) (**Figure 8D**). Yet, measured total sulfide concentrations from day 0 to day 20 could only explain 1.5% of the decrease of porewater SO_4^{2-} in the 6.0 ppt treatment and up to 10% in the 0.5 ppt treatment.

Incubation peat cores were filled with treatment water containing 5.5 mg C L^{-1} DOC with a DOM $SUVA_{254}$ value of 4.24 L mg C^{-1} m^{-1} and spectral slope ratio (S_R) of 0.86. In comparison, Day 0 porewater samples, across the five treatments, exhibited significantly higher DOC concentrations (11.9-33.4 mg C L^{-1}), lower DOM $SUVA_{254}$ values (0.69 – 2.41 L mg C^{-1} m^{-1}), and higher S_R values (1.01-2.71) (**Figure 9**). Measurements of DOC concentration at each treatment (**Figure 9A**) through time do not show significant trends nor do any treatments statistically differ from the 0.16 ppt freshwater control ($p>0.05$, Dunnett, n = 105). Although the DOC concentration varied considerably for the incubated porewaters across the experiment (10-165 mg C L^{-1}) and exceed that of the typical observed[28] porewater DOC concentration at WCA site 3A-H (17-23 mg C L^{-1}), these elevated DOC concentrations are not atypical of porewaters of other more nutrient impacted sites in the Florida Everglades[28] and SO_4^{2-}-rich peatlands.[40] Furthermore, the DOC concentrations measured were highly variable both within salinity treatments and between replicate incubation cores, suggesting that the carbon pool in these incubation cores is highly dynamic, susceptible to rapid changes in concentration, and may reflect heterogeneity in the peat cores. A previous incubation study of sea-level rise in the Florida Everglades identified increased innundation of peat as a driver of

increased porewater DOC with concomitant declines in soil bulk density, however, they found that increased salinity alone did not result in increased porewater DOC.[41] Other studies in peatlands experiencing sea-level rise have also reported that increased salinity decreases DOC production.[42–44] Yet, under the conditions of this study with fresh peat cores, the short-term response due to salinity increases was an increase in porewater DOC concentration, likely due to microbial mobilization of peat carbon, fueled by increases in SO_4^{2-} reduction.

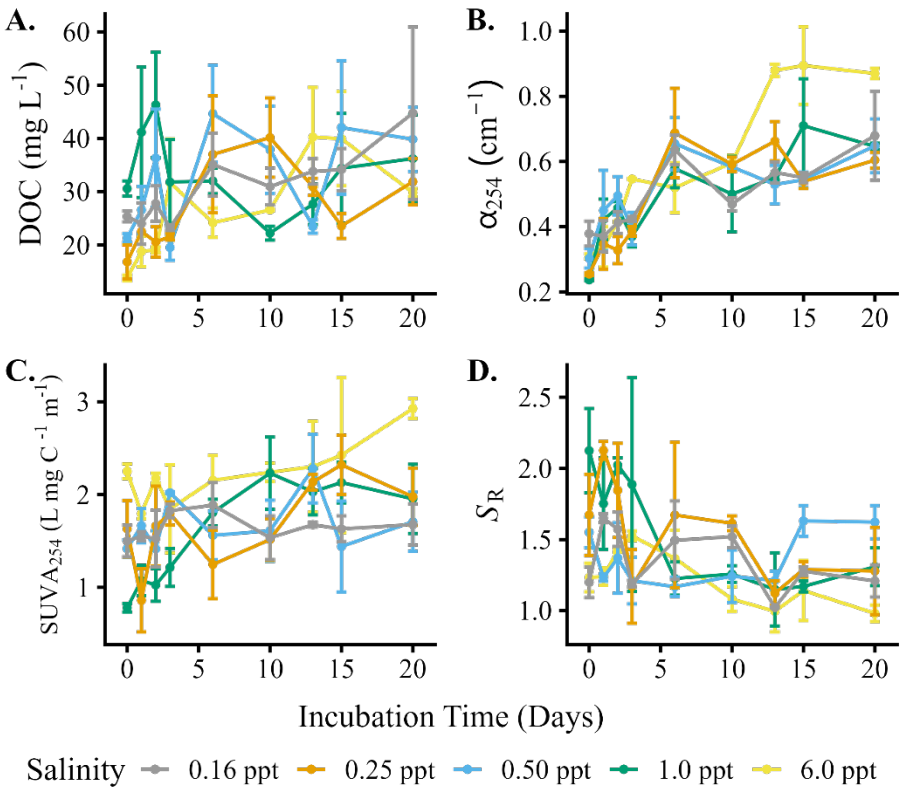

Figure 9. Porewater (A) dissolved organic carbon (DOC) concentration, (B) decadic abosorbance coefficient at 254 nm (α_{254}), (C) dissolved organic matter (DOM) specific UV absorbance at 254 nm ($SUVA_{254}$), and (D) spectral slope (S_R) through time for each treatment group. Colored lines represent different treatment salinities. Outliers in DOC concentration removed above 80 mg C L^{-1} for clarity in graph.

Trends in DOM optical data with increased incubation time were clearer than DOC concentration. Decadic absorbance at 254 nm (α_{254}), a measurement which is influenced both by DOC concentration and DOM aromaticity, shows consistent monotonic increases through time across all salinity treatments (**Figure 9B**), with the 6.0 ppt treatment demonstrating statistically higher mean α_{254} than every other salinity

treatment from day 10 onwards (Tukey, $p < 0.05$, $n = 40$). DOM $SUVA_{254}$ measurements generally increased with incubation time for each treatment (**Figure 9C**), indicate increasing aromaticity of the carbon pool through time. This trend is most evident in the 1.0 ppt treatment, where the DOM $SUVA_{254}$ increased from 0.78±0.05 L mg C^{-1} m^{-1} on day 0 to 2.0 ± 0.4 L mg C^{-1} m^{-1} on day 20. The 6.0 ppt salinity group also demonstrates higher $SUVA_{254}$ values throughout the 20-day experiment and was the only treatment to statistically differ from the control 0.16 ppt treatment ($p < 0.001$, Dunnett, $n = 105$). Further, spectral slope ratio (S_R), an optical metric that scales negatively with DOM molecular weight,[37] showed a consistent, monotonic decrease with increased incubation time across treatment salinities (**Figure 9D**). This was most noticeable in the 0.25, 1.0, and 6.0 ppt treatments, indicating through proxy that the DOM pool increased in molecular weight through time. The particularly high S_R values, and low $SUVA_{254}$ values, at the 1.0 ppt treatment during the first few days of incubation suggest the presence of low molecular weight, aliphatic DOM. Low molecular weight organic acids, which are non-absorbing and can exhibit unique dynamics in soil incubation experiments,[45,46] were not measure and could have influenced trends in DOC concentration (and thus $SUVA_{254}$). Together, the trends in DOM optical indices suggest that, compared to the low salinity control, the DOM pool in the four higher salinity amendments becomes more enriched in higher molecular weight molecules through time as low molecular-weight and aliphatic DOM molecules are mineralized.

We interpret that the concentration dynamics of filter-passing total Fe, SO_4^{2-}, and total sulfide in porewaters were driven by microbial processes and potential Fe-S and DOC interactions. Previous research[41] has demonstrated that across the Everglades, nearly all the exchangeable Fe on Everglades peat sediments, under reducing conditions, is present as Fe(II). Iron speciation in pore waters were modeled (MINEQL+) and under all ionic strengths and ORP conditions at day 20 porewater Fe was present as reduced Fe(II) independent of salinity. The reductive dissolution of Fe(III) from solid peat sediment is likely to explain the significant increase in Fe concentrations at the 6.0 ppt treatment, which demonstrates strong correlation between ORP and Fe concentrations in porewaters, however, the 1.0 ppt treatment which demonstrates lower ORP than the 6.0 ppt treatment, demonstrates the lowest porewater Fe concentrations.

Thus, we conclude that it is unlikely that the increases in filter-passing total Fe at 6.0 ppt with increased incubation time, compared to the other salinity treatments, was due to reductive dissolution of Fe(III) mineral species. We further propose that the mobilization of Fe was largely independent of cation exchange from ions in the treatment waters, as this would be expected to be observed at t = 0 days and all five salinity treatments exhibited similar concentrations of filter-passing total Fe at t=0 days. Rather, the data support that porewater concentrations of filter-passing Fe were due to the co-release of DOC and Fe(II) bound from the solid peat phase and perhaps weakening of activity coefficients and increased K_{SP} values of Fe-sulfide ($FeS_{(s)}$) minerals at high ionic strengths. First, at each salinity, there is a positive correlation between DOC and filter-passing total Fe concentration (**Figure 10**) at the 0.25, 0.50, and 6.0 ppt salinity groups independently (0.25 ppt: $p < 0.001$, 0.50 ppt: $p<0.05$, 6.0 ppt: $p<0.001$, Pearson). The 1.0 ppt treatment, conversely, did not show strong correlation between DOC and filter-passing total Fe for reasons detailed below. Secondly, MINEQL+ modelling suggests Fe sulfide ($FeS_{(s)}$) minerals are more soluble with increasing ionic strength (**Figure 11**). Thus, it is likely that Fe(II) was co-mobilized from peat sediments due to microbial activity over the 20 days, with a minor impact of ionic strength on the solubility of $FeS_{(s)}$.

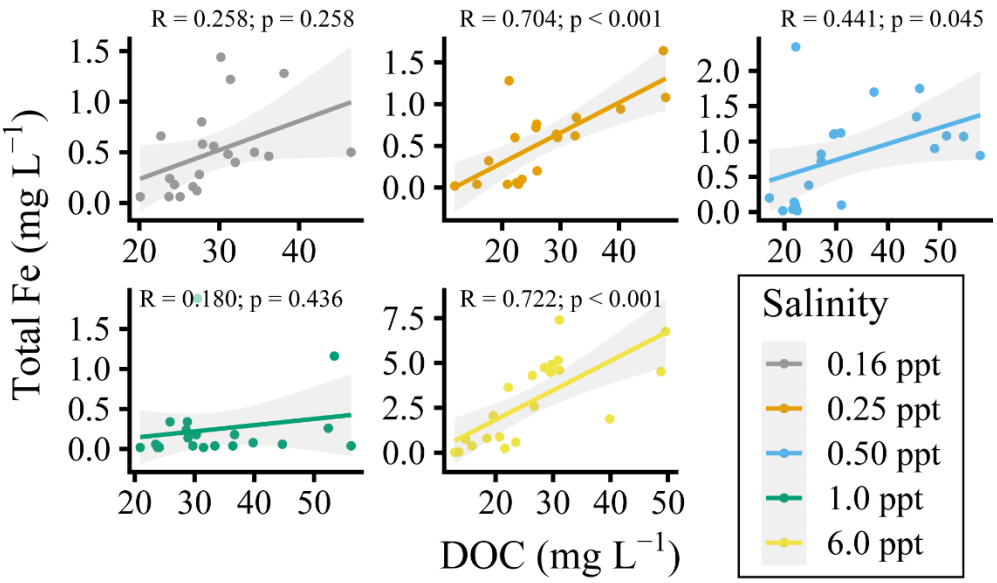

Figure 10. Total filter-passing Fe concentrations (y-axis) plotted against DOC concentration (x-axis). Colors represent various salinity treatment groups. Solid colored line represents linear trend model and shaded regions represent standard error of the models. Significance is indicated by magnitude of p-value (Pearson).

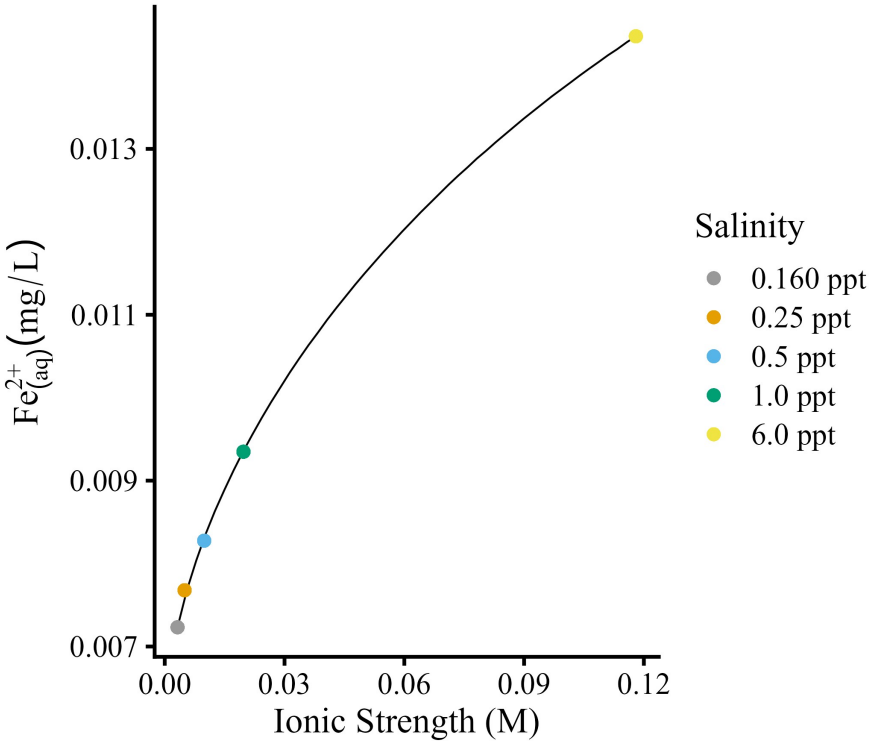

Figure 11. Modelled Fe(II) response to increased ionic strength from MINEQL+. Line represents modelled concentrations of aqueous Fe(II) and points represent endmember salinities.

The decreases in SO_4^{2-} and ORP and increases in sulfide concentration in peat incubations demonstrate that the microbial communities in the peat cores quickly deplete oxygen and switch to dissimilatory SO_4^{2-} reduction to drive anaerobic respiration. The sulfur mass balance analysis, which showed that the majority of SO_4^{2-} that was reduced was not present as total sulfide, is likely due to a combination of processes including the precipitation of $FeS_{(s)}$ and (to a lesser degree) Hg-sulfide minerals,[47–49] removal of sulfur during DOM sulfurization processes,[27] and evasion of $H_2S_{(g)}$. We suspect that at the 1.0 ppt treatment, the high concentration of sulfide resulted in precipitation of $FeS_{(S)}$, suppressing porewater filter-passing total Fe concentrations due to higher levels of SO_4^{2-} reduction at the 1.0 ppt than other treatments. The overall findings demonstrate that higher salinity water, which has higher SO_4^{2-}, stimulates SO_4^{2-}-reducing bacteria leading to elevated concentrations of sulfide, lower ORP, and more aromatic DOM.

Mercury Methylation

A mass balance analysis of total ^{201}Hg in each core was determined, for each treatment salinity and each time point (**Figure 12A**), demonstrating that the total amount of ^{201}Hg(II) tracer added to each core was variable. The variability between cores is interpreted to be due to the process by which core were filled (**Figure 3**), with the cores that were filled first scavenging ^{201}Hg(II) from porewaters while cores were being flushed with the incubation water. Thus, within each salinity treatment, cores that were filled last received porewater which had a modestly lower concentration of ^{201}Hg(II). On average, cores received 302 ± 30 ng ^{201}Hg(II) (mean ± standard error) at the start of the experiment and were not statistically different between the five salinities (one-way ANOVA, $p>0.1$, $n = 80$). To account for the differences in the amount of amended ^{201}Hg(II) tracer added to each core, results are presented as a percentage of total ^{201}Hg tracer within each core. The peat binding capacity for Hg(II) was not saturated due to the high levels of ambient total Hg on the peat cores (7,805± 269 ng), finding that the mass of ambient Hg(II) + ^{201}Hg(II) do not statistically differ from the ambient Hg in the cores (Welch two sample t-test, $p > 0.45$).

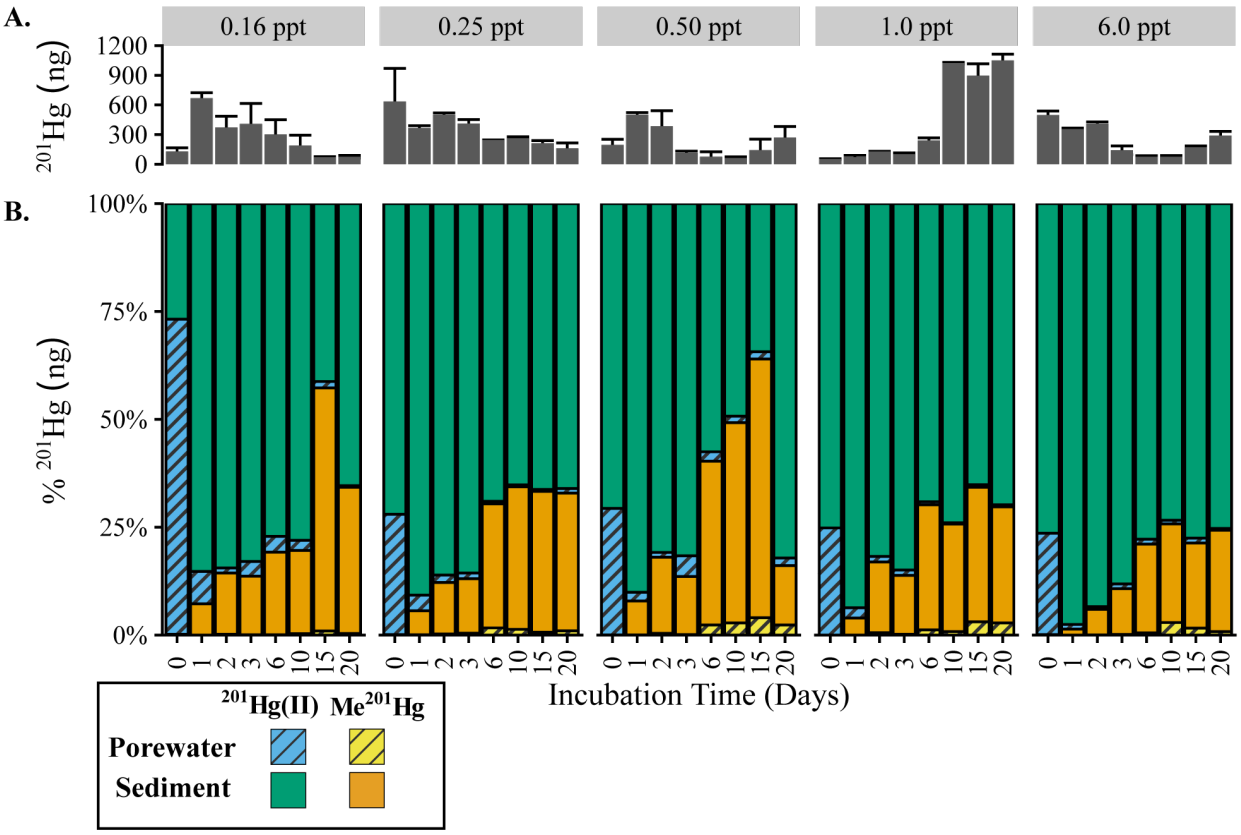

Figure 12. (A.) Total mass of ^{201}Hg added to incubation cores. Bar represents mean of replicate cores and error bar represents standard error of the mean. (B.) Total ^{201}Hg by Hg species and location. Yellow and orange bars represent Me^{201}Hg, green and blue bars represent ^{201}Hg(II). Percentages are the means of replicate incubations. Hashed bars represent porewater ^{201}Hg species, solid bars represent peat ^{201}Hg species.

To assess the impact of salinity on ^{201}Hg(II) methylation, the partitioning of the ^{201}Hg(II) tracer in the cores was first evaluated. **Figure 12B** presents the proportions of porewater and peat ^{201}Hg species (Me^{201}Hg and ^{201}Hg(II)) as a percentage of the total ^{201}Hg(II) with increased incubation time. The concentration data of Me^{201}Hg and ^{201}Hg(II) in the porewater and in the peat with increased incubation time are presented in **Figure 13**. From day 0 to day 1, porewater ^{201}Hg(II) concentration declined in each of the five salinity treatments, while concurrent increases in sediment ^{201}Hg(II) concentration were observed; these results show the rapid but incomplete partitioning of the ^{201}Hg(II) tracer to the peat within the first day of the experiment. Me^{201}Hg was near or below the detection limit at t = 0 days, as the incubation water only contained ^{201}Hg(II). At t = 1 day, Me^{201}Hg production was detectable and was lowest in the 1.0 and

6.0 ppt treatments compared to the three lower salinity treatments (0.16-0.5 ppt). The 6.0 ppt treatment exhibited the lowest level of $^{201}Hg(II)$ methylation to $Me^{201}Hg$ until day 6, when the total methylation at 6.0 ppt reaches 21%. The 0.16 (control) and 0.5 ppt treatments reached maximum levels of methylation across the entire experiment, with day 15 and 10 total methylation percentages of 64% and 49% respectively at 0.5 ppt, and a day 15 total methylation percentage of 57% at 0.16 ppt. The 6.0 ppt group demonstrated the lowest $Me^{201}Hg$ production by day 15, with total methylation percentage of 21%. These values for total methylation in incubated Everglades cores are significantly higher than previously recorded literature ranges for Everglades peat methylation percentages, which typically range from 1-8% over 24 hours,[8,12,50] likely due to the 20-day duration of experiments. Overall, there were no statistical differences between salinity treatments with regards to total $^{201}Hg(II)$ methylation (one-way ANOVA, $p>0.05$, $n = 80$), however, in each of the elevated salinity treatments (0.25-6.0 ppt), $Me^{201}Hg$ was observed to accumulate in porewaters, as indicated by yellow hashed bars in **Figure 12B**.

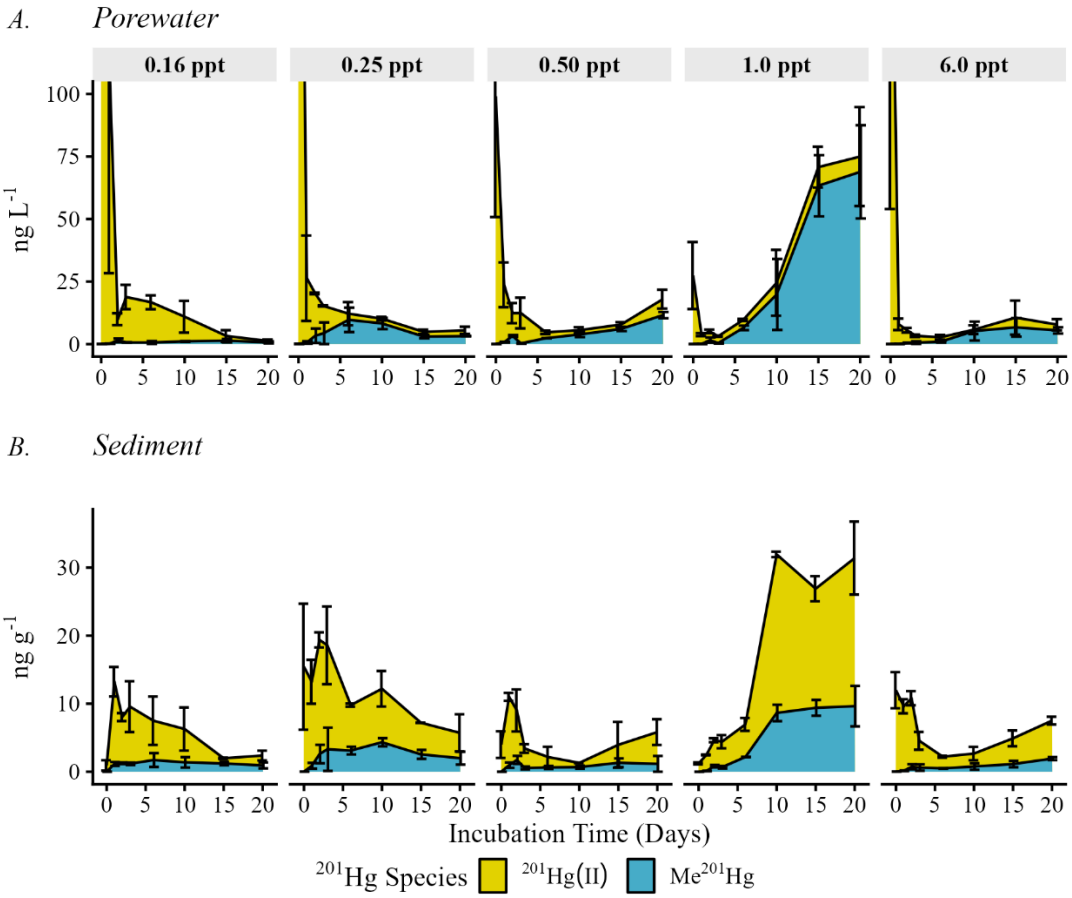

Figure 13. Porewater (A) and sediment (B) methylmercury ($Me^{201}Hg$) (blue) and total inorganic $^{201}Hg(II)$ tracer concentrations (yellow) in incubated peat cores at 0.16 ppt (left) and 1.0 ppt (right). Data points present average values of experimental duplicates and error bars represent the standard error of the mean.

The net efficiency of Hg(II) methylation in the porewater was determined by quantifying the percentage of total porewater ^{201}Hg tracer that had been converted to $Me^{201}Hg$ at each time point (**Figure 14**). For the 0.16 ppt treatment, the methylation efficiency was comparatively low from 0-10 days, increased from 10-15 days, and plateaued between 15-20 days. In contrast, the 0.25,0.5,1, and 6 ppt treatments exhibited increasing methylation efficiencies from day 0-10 and plateaued from days 10-20. Methylation efficiencies suggest that at elevated salinity the methylation of $^{201}Hg(II)$ was enhanced in porewaters compared to the 0.16 ppt. Maxima in net $^{201}Hg(II)$ methylation (mean ± standard error) was 75±16% for the 0.25 ppt treatment on day 10, 72±2% for the 0.5 ppt treatment on day 15, 85±1% for the 1.0 ppt treatment on day

20, and 72±39% for the 6.0 ppt treatments on day 10. In contrast, the 0.16 ppt treatment exhibited lower methylation efficiency in porewaters through time and reaches a maximum of 51±16% on day 15. At time points beyond 3 days, each elevated salinity had a statistically higher methylation efficiency percentages compared to the 0.16 ppt freshwater treatment (Dunnett, $p < 0.05$, $n = 40$). There was no statistical pairwise differences between the four elevated salinities (Tukey, $p > 0.05$, $n = 40$). The high percentages of porewater ^{201}Hg(II) methylation observed in elevated salinity treatments highlights that accumulation of MeHg in porewaters is strongly controlled by the availability of dissolved inorganic Hg(II) in porewaters and the aqueous complexation of produced MeHg.

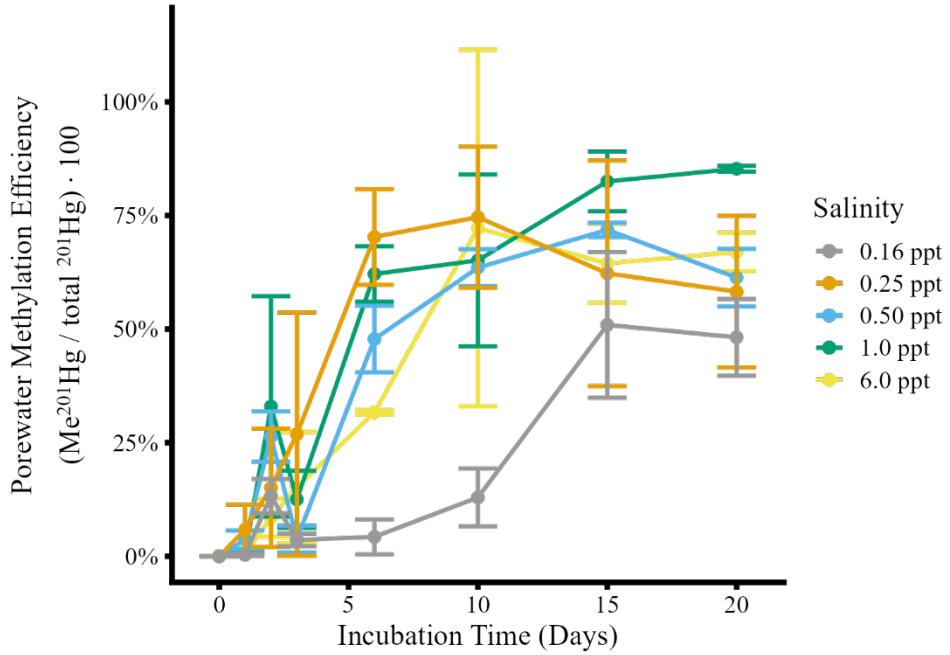

Figure 14. Porewater methylation efficiency presented as percent of total porewater ^{201}Hg as Me^{201}Hg. Data points present average values of experimental duplicates and error bars represent the standard error of the mean.

Distribution coefficients (K_d) of total ^{201}Hg, ^{201}Hg(II), and Me^{201}Hg were quantified across each treatment through time (**Figure 15**) to determine salinity effects on partitioning of Hg species between peat sediment and porewater. Across all salinity treatments, K_d values for both total ^{201}Hg (**Figure 15A**) and ^{201}Hg(II) (**Figure 15B**) increase rapidly from day 0, governed by the ability of peat soils to rapidly bind inorganic Hg(II). Altogether, no statistical differences were observed between salinities in the partitioning

of Hg(II) to the porewaters. For $Me^{201}Hg$ (**Figure 15C**), however, K_d values decreased with increased incubation time for each salinity, but most drastically in the 0.5, 1.0, and 6.0 ppt salinity treatments. By day 15, each of those treatments reached mean $Me^{201}Hg$ log K_d values of 2.28 ± 0.17, 2.18 ± 0.14, and 2.26 ± 0.08 respectively, compared to 3.00 ± 0.19 and 2.92 ± 0.01 for the 0.16 and 0.25 ppt treatments. By days 15 and 20, the 1.0 ppt treatment reached the lowest mean log K_d values of all treatments (2.18±0.14 and 2.14±0.02 respectively). When examining $Me^{201}Hg$ log K_d values at time ≥ 3 days (due to the variability of 0-2 day time points), the 0.5 ppt treatment demonstrates the lowest mean log K_d value (2.31 ± 0.05), followed by the 1.0 ppt treatment (2.41 ± 0.12) and the 6.0 ppt treatment (2.45 ± 0.09). There was a statistical difference between salinity treatment 0.16 ppt and treatments 0.25, 0.5, 1.0, and 6.0 ppt (Dunnet, $p < 0.001$, $n = 80$), as well as statistical differences between the 0.5 ppt and 0.25 ppt treatments (Tukey, $p < 0.05$, $n = 80$). These results show that at elevated levels of salinity, newly formed MeHg in inundated peat has a greater distribution in porewaters, with evidence that moderate salinity intrusion of 0.5 ppt having the largest effect.

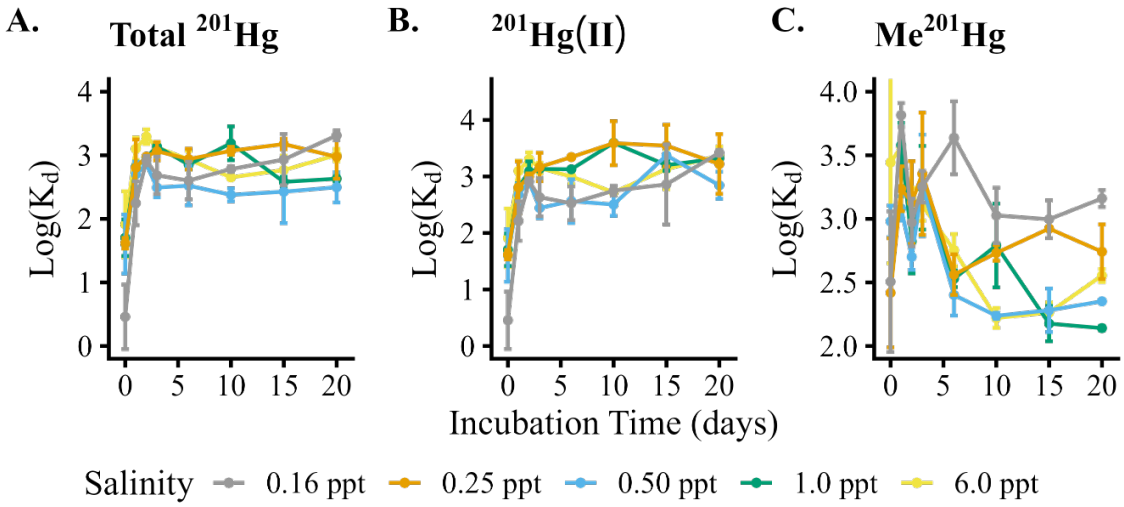

Figure 15. Distribution coefficients presented as Log(K_d) through time for (A) the total ^{201}Hg tracer, (B) inorganic $^{201}Hg(II)$ fraction, and (C) the $Me^{201}Hg$ fraction of spiked isotope tracer. Data points present average values of experimental duplicates and error bars represent the standard error of the mean.

Drivers of Mercury Methylation

Our findings suggest that at moderate salinity levels common at the onset of saltwater intrusion, Florida Everglades peat demonstrate the ability to methylate Hg(II) at similar levels as peat receiving freshwater inputs. However, as evidenced by $Me^{201}Hg$ K_d (**Figure 15C**) and methylation efficiency rates (**Figure 14**), at elevated salinities (0.25-6.0 ppt) a greater proportion of the MeHg formed is stabilized in porewaters compared to the low salinity, freshwater treatment, where MeHg was primarily bound to the peat. Concomitant with porewater MeHg production, we observed increases in porewater α_{254} indicating elevated concentrations or increases in aromatic DOM through time across each treatment, as well as increases in porewater sulfide concentrations at higher salinities, both of which are important aqueous ligands for $^{201}Hg(II)$ complexation and bioavailability to methylation as well as for complexation and stabilization of $Me^{201}Hg$ in pore water.

Linear regression and Pearson correlation analyses between porewater $^{201}Hg(II)$ methylation efficiency and pertinent parameters of geochemical ligands (total sulfide concentration, DOC concentration, DOM $SUVA_{254}$, and α_{254}) provide evidence of the underlying reasons for increase MeHg presence in porewater of higher salinity treatments (**Figures 16, 17**). First, we observed that at each elevated salinity treatment, there were strong positive correlations between sulfide concentrations and porewater $^{201}Hg(II)$ methylation efficiency (Pearson, $p<0.05$) as well as between sulfide and porewater $Me^{201}Hg$ concentrations (Pearson, $p<0.002$) (**Figure 16B-16E**). At the 1.0 ppt treatment, which displays the strongest positive trends between sulfide and MeHg and methylation efficiency (**Figures 16D**, **17A**, and **17B**), we also observe strong coupling of sulfide concentrations and total ^{201}Hg concentrations. Second, DOM concentration and composition was also a controlling factor in influencing Hg(II) methylation. Across all five salinities, decadic absorbance coefficient at 254 nm (α_{254}) (which encompasses both DOC concentration and aromaticity) correlated positively with porewater $Me^{201}Hg$ concentrations and porewater $^{201}Hg(II)$ methylation efficiency at each of the elevated treatment salinities (**Figure 16B-16E)**. In contrast, the DOC concentration or DOM $SUVA_{254}$ could not explain these differences across all treatments, likely due to

confounding effects of sulfide or additional variables not captured in this study. Third, distribution coefficients of $Me^{201}Hg$ provide a direct measurement of MeHg partitioning to peat sediments and support MeHg stabilization in porewaters by aqueous ligand complexation. From salinity 0.50 ppt to 6.0 ppt, however, Log K_d for $Me^{201}Hg$ demonstrates statistically significant negative correlations with DOM α_{254}, and S^{2-} concentration (**Figures 16C**, **16D**, and **16E**). The majority of the observed correlations between concentrations and parameters of aqueous ligands (e.g. porewater sulfide concentrations, DOC concentrations, DOM α_{254}) and porewater $^{201}Hg(II)$ methylation efficiency (% methylation) were also observed for porewater $Me^{201}Hg$ concentrations. This finding gives confidence that trends in the porewater concentration data presented in **Figure 13A** are not merely an artifact of the total amount of ^{201}Hg tracer loaded onto the individual incubation cores, but rather, represent trends independent of the experimental conditions of each core. Taken together, these observations support that elevated SO_4^{2-} at salinities 0.5-6.0 ppt result in increased concentrations of aqueous ligands (DOM, sulfide) that enhance the production of MeHg that is present in pore waters.

Porewater Pearson Corellation Matrices

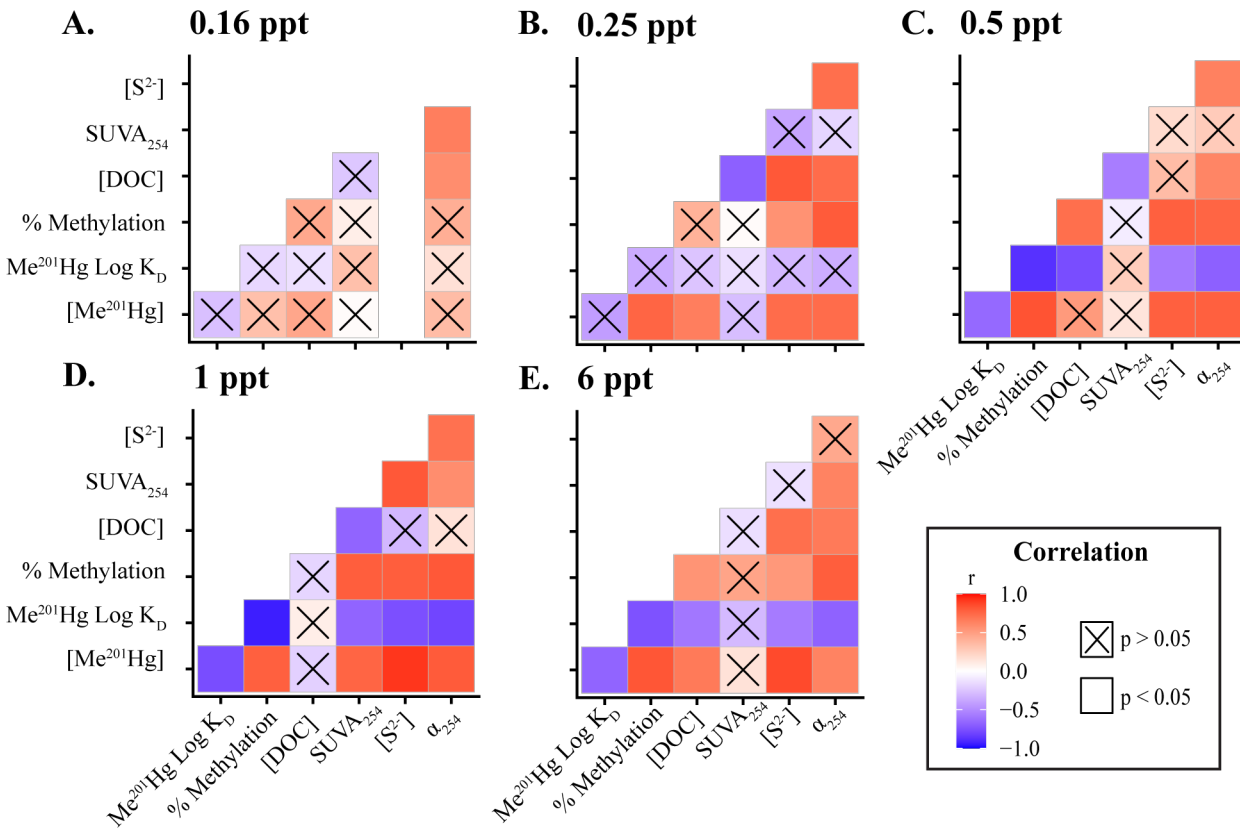

Figure 16. Pearson correlation matrices for porewater samples from treatment salinities (A – E) 1.0 ppt – 6.0 ppt. Darker red boxes at intersection between two parameters indicates stronger positive correlation; darker blue boxes represent stronger negative correlation. Boxes at intersections between two significantly statistically correlated parameters (Pearson, $p < 0.05$) are represented as an open box. Boxes at intersections between two insignificantly statistically correlated parameters (Pearson, $p > 0.05$) are represented by a box with a black X symbol. S^{2-} concentration correlations are omitted from panel A due to S^{2-} being below detection limit in all but one core at 0.16 ppt.

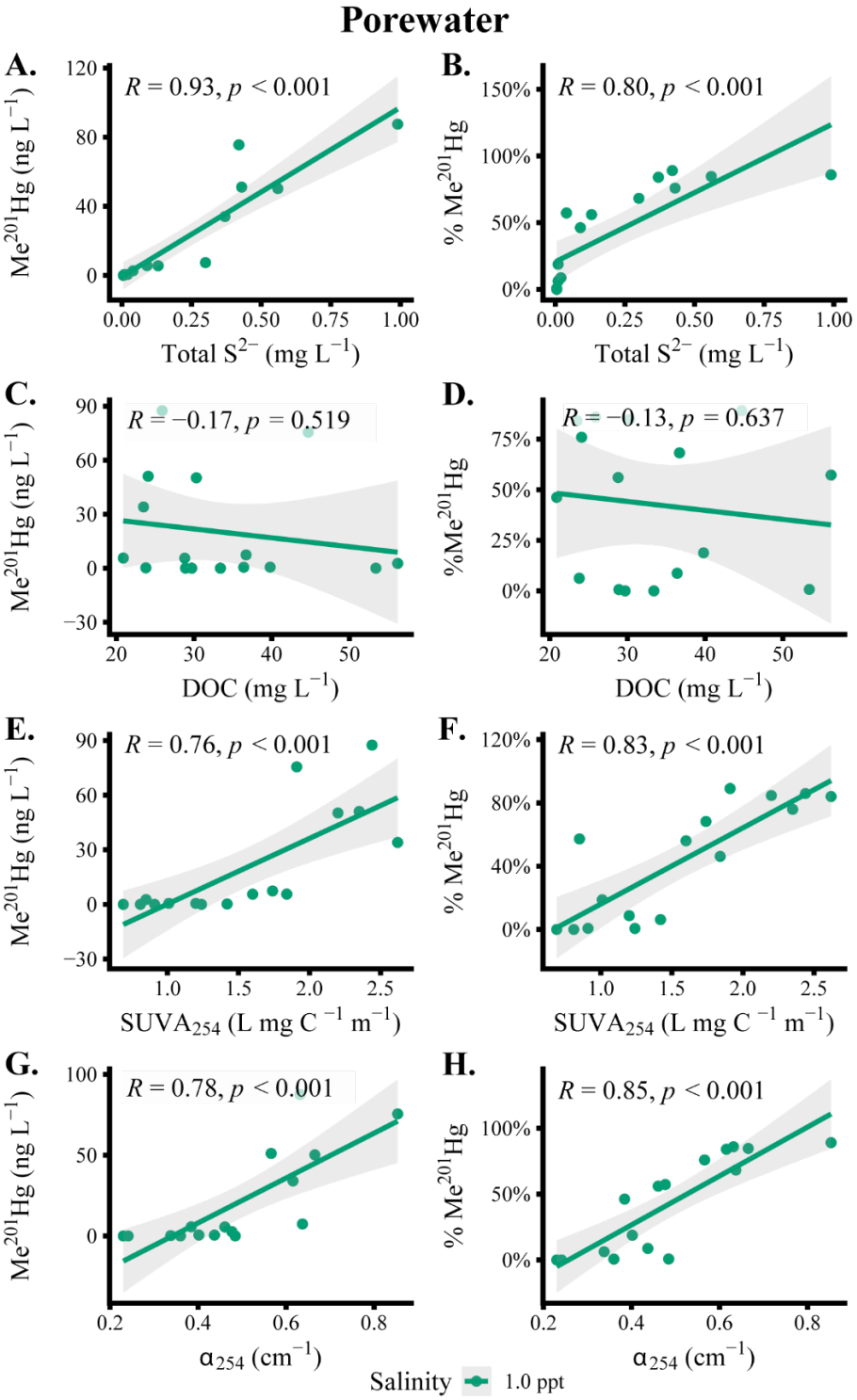

Figure 17. Scatter plots for the 1.0 ppt salinity treatment with total sulfide (S^{2-}), dissolved organic carbon (DOC), specific UV absorbance at 254 nm ($SUVA_{254}$) and decadic absorbance coefficient at 254 nm (α_{254}) on the x axes, and $Me^{201}Hg$ concentration and $^{201}Hg(II)$ methylation efficiency on the y axes. Points represent individual core incubations. Solid green line presents linear trend line, and shaded gray area presents 95% confidence interval. Pearson's R and p value statistics are provided on each scatter plot.

The mechanistic processes responsible for the enhanced Hg(II) methylation and stabilization of porewater MeHg at higher salinities is likely linked directly or indirectly to the multifaceted role of SO_4^{2-}, microbial processes, and occurrence or availability of aqueous Hg(II) and MeHg ligands. At elevated salinity, we observed evidence of SO_4^{2-} reduction through the detection of S^{2-} (**Figure 8D**) and lower ORP values (**Figure 8A**) compared to the control as well as a strong correlation between increased sulfide and porewater MeHg production. Taken together, this indicates that dissimilatory SO_4^{2-} reduction was either directly impacting Hg(II) methylation through coupling of dissimilatory SO_4^{2-} reduction to the microbial methylation of ^{201}Hg(II) in salinity impacted porewaters, or indirectly influencing MeHg production through sulfide binding Hg(II), increasing its bioavailability, or indirectly through increasing DOC concentration and aromaticity of DOM.

The ability of microbes in Everglades peat has previously been shown to make a rapid switch to dissimilatory SO_4^{2-} reduction as the primary pathway of anaerobic respiration in peat experiencing salinity intrusion;[31,42] it is unclear, however, if the SO_4^{2-} reducing bacteria are directly or indirectly involved in the methylation.[8] There was evidence that sulfide increased ^{201}Hg(II) bioavailability by influencing the availability of total ^{201}Hg at the 1.0 ppt treatment and it is likely that sulfide in porewaters of the 1.0 ppt treatment influenced the formation of highly bioavailable Hg-S-DOM complexes under mildly sulfidic conditions.[51] Previous research has shown that in coastal marshes, along salinity transects, sulfur content in DOM increases due to increased sulfide production, and is also in agreement with Everglades research suggesting DOM sulfurization occurs within porewaters at SO_4^{2-} impacted sites.[22] Altogether, the trend of increasing sulfide correlating with increased porewater Hg(II) methylation further agrees with previous Florida Everglades work which suggests that elevated SO_4^{2-} in the freshwater Everglades from agricultural runoff stimulates SO_4^{2-} reduction, sulfide accumulation, and increased Hg(II) methylation.[22,52] In the 0.16 ppt freshwater control, SO_4^{2-} levels were not high enough to support sustained dissimilatory SO_4^{2-} reduction, evident by undetectable levels of sulfide in core porewaters. This presumably contributes to the

significantly lower porewater Hg(II) methylation efficiency observed in the 0.16 ppt control, as methanogens have been proposed to be less efficient Hg(II) methylators.[53] The increase in SO_4^{2-} reduction rates also served to increase the rates of anaerobic respiration and carbon mineralization of solid peat organic matter and DOM. This increase in carbon mineralization is evident in both the 1.0 and 6.0 ppt treatments which see significant increases in both $SUVA_{254}$ (**Figure 11C**) and α_{254} (**Figure 11B**) through time, indicating that at those treatment, the dissolved carbon pool is becoming more aromatic as it is being mineralized. This would serve to both (1) retain porewater Hg(II) by complexing Hg(II) and subsequently increasing its bioavailability for methylation[8,17,19,54] as evidenced by strong positive correlations between SUVA and total ^{201}Hg at the 1.0 ppt treatment, as well as to (2) stabilize produced MeHg in porewaters compared to the control. This is evidenced by the strong trends observed at each of the elevated salinity treatments between α_{254} and $Me^{201}Hg$ concentrations and porewater Hg(II) methylation efficiency. Our results agree with previous work which determined distribution coefficients for Hg(II) between Everglades peat substrate and water ($10^{21.8}$ – $10^{22.0}$ M^{-1}) and DOM and water ($10^{22.8}$ – $10^{23.2}$ M^{-1}), indicating stronger binding of Hg(II) to DOM than Everglades peat.[55] MeHg has also been demonstrated to strongly bind to DOM, with conditional stability constants for MeHg-DOM ranging from 10^{12}-$10^{16.5}$ further confirming the importance of DOM on porewater MeHg stabilization observed at higher salinities in this experiment.[56–58]

Conclusions

Our results have several implications for sea-level rise in the Florida Everglades and other coastal peatlands. As sea level rises, and previously freshwater wetland peat are inundated with increasingly saline waters, our results suggest that salinity will affect Hg cycling across many natural salinity regimes in both the short and long term. Due to the gentle elevation gradient of Shark River Slough and the southern Florida Everglades, extensive areas of coastal wetlands can be inundated during wind and storm driven surges and during seasonal fluctuations when the freshwater hydraulic head is weakened. These events will be exacerbated by rising sea levels due to climate change.[59] For previously freshwater peat that will begin to

experience small tidal pulses of seawater salinity, our findings suggest that Hg(II) methylation will begin within one day in salinity conditions up to 6.0 ppt. Previous research in the Shark River Slough estuary of the Florida Everglades has identified the release and tidal transport of MeHg complexed to DOM released from peat as a significant source of MeHg to coastal waters.[5]Further research in the Taylor Slough of the Florida Everglades indicates sediments in mangrove transition zones as having high Hg(II) methylation potentials[60] providing further evidence that tidal pumping of MeHg is poised to be a prominent driver of export of MeHg to coastal waters. Our work suggests that even a brief influx of SO_4^{2-} from seawater to peat previously flooded with freshwater from a tidal event or storm surge could stimulate methylation of Hg(II) in porewaters. Under tidal conditions, any produced MeHg that remains in the porewater could then be transported to coastal waters through tidal pumping.

These findings are relevant for tidal wetlands globally. Work in a Chesapeake Bay salt marsh has identified the salt marsh as a small net exporter of both total dissolved Hg and MeHg and a sink for particulate Hg.[61,62] Further research in Sepetiba Bay, Brazil, highlighted porewaters with high Hg concentrations draining out of mangrove transition zones.[63] Overall, we expect that the ability of estuarine sediments to bind MeHg will strongly influence the export of MeHg from estuaries to coastal waters. While K_d values for $Me^{201}Hg$ in our incubations remained high during early time points, which may allow produced MeHg to bind strongly to peat, previous work in tidal lagoons in Italy has demonstrated that shear forces due to tidal flooding can increase diffusion or advection of dissolved Hg species from surficial sediments and promote *in situ* production of MeHg or desorption of both Hg species from sediment particles due to oxidative dissolution of redox sensitive sulfide minerals.[64]

In our study, at the higher salinity level of 6.0 ppt, the methylation response was demonstrably slower (**Figure 12B**), likely due to microbial communities adjusting to increased osmotic pressure, which may also slow the production of MeHg in peat due to short-term pulses in salinity from tidal cycling.[30,65] The slower response of the 6.0 ppt treatment is further confirmed by lag in sulfide concentration at the 6.0 ppt treatment (**Figure 8D**), indicative of diminished SO_4^{2-} reducing bacteria activity through 6 days. This suggest

diminished capabilities for MeHg export at higher salinities in the short term, relevant for brief surges of salinity due to storm surge, for instance. In the long term, however, peat core incubations experiencing salinity intrusion up to 6.0 ppt demonstrate the ability to methylate Hg(II) at similar rates to lower salinities. The lowered K_d values for $Me^{201}Hg$ (**Figure 15C**) at higher salinities observed in this experiment indicate that MeHg produced due to long term salinity intrusion will more strongly partition to the porewaters. The implications of higher porewater MeHg concentrations are significant as dissolved free MeHg enters the food web through accumulation of MeHg in periphyton and phytoplankton in the water column,[24–27] thus the increased partitioning of MeHg from peat sediments to surrounding porewaters due to increased salinity would plausibly be a driver of MeHg bioaccumulation in coastal ecosystems. Previous work has shown that MeHg bioaccumulation and biomagnification is most drastic in coastal ecosystems proximal to freshwater inputs[66] and dolphins from the Florida Keys and coastal Everglades have been shown to have the highest levels of THg in any dolphins recorded in the southeastern USA.[67] Overall the production and export of toxic MeHg from the freshwater Everglades to coastal ecosystems in the long term will ultimately pose an issue for the health of Florida's coastal ecosystems and fisheries. This study highlights the need for studies of Hg(II) methylation *in-situ* along tidally influenced salinity gradients in coastal wetlands at high spatial and temporal resolution, with an emphasis on salinity fluctuations from tidal cycles, storm surges, or changes in seasonal freshwater delivery.

Bibliography

(1) United Nations Environment Programme. *GLOBAL MERCURY ASSESSMENT*; 2018.

(2) Hsu-Kim, H.; Kucharzyk, K. H.; Zhang, T.; Deshusses, M. A. Mechanisms Regulating Mercury Bioavailability for Methylating Microorganisms in the Aquatic Environment: A Critical Review. *Environ Sci Technol* **2013**, *47* (6), 2441–2456. https://doi.org/10.1021/es304370g.

(3) Wiener, J.; Krabbenhoft, D.; Heinz, G.; Scheuhammer, A. Ecotoxicology Of Mercury. In *Handbook of Ecotoxicology, Second Edition*; CRC Press, 2002. https://doi.org/10.1201/9781420032505.ch16.

(4) Lange, T.; Rumbold, D. G.; Frederick, P. C.; Cunningham, M.; Pollman, C. D. Temporal Changes in Mercury Concentrations in Everglades Biota. In *Mercury and the Everglades. A Synthesis and Model for Complex Ecosystem Restoration*; Springer International Publishing: Cham, 2020; pp 27–50. https://doi.org/10.1007/978-3-030-55635-8_2.

(5) Bergamaschi, B. A.; Krabbenhoft, D. P.; Aiken, G. R.; Patino, E.; Rumbold, D. G.; Orem, W. H. Tidally Driven Export of Dissolved Organic Carbon, Total Mercury, and Methylmercury from a Mangrove-Dominated Estuary. *Environ Sci Technol* **2012**, *46* (3), 1371–1378. https://doi.org/10.1021/es2029137.

(6) IPCC. *Climate Change 2021 The Physical Science Basis Summary for Policymakers Working Group I Contribution to the Sixth Assessment Report of the Intergovernmental Panel on Climate Change*; 2021.

(7) Zhang, K. Analysis of Non-Linear Inundation from Sea-Level Rise Using LIDAR Data: A Case Study for South Florida. *Clim Change* **2011**, *106* (4), 537–565. https://doi.org/10.1007/s10584-010-9987-2.

(8) Peterson, B. D.; Krabbenhoft, D. P.; McMahon, K. D.; Ogorek, J. M.; Tate, M. T.; Orem, W. H.; Poulin, B. A. Environmental Formation of Methylmercury Is Controlled by Synergy of Inorganic Mercury Bioavailability and Microbial Mercury-methylation Capacity. *Environ Microbiol* **2023**, *25* (8), 1409–1423. https://doi.org/10.1111/1462-2920.16364.

(9) Poulin, B. A.; Ryan, J. N.; Tate, M. T.; Krabbenhoft, D. P.; Hines, M. E.; Barkay, T.; Schaefer, J.; Aiken, G. R. Geochemical Factors Controlling Dissolved Elemental Mercury and Methylmercury Formation in Alaskan Wetlands of Varying Trophic Status. *Environ Sci Technol* **2019**, *53* (11), 6203–6213. https://doi.org/10.1021/acs.est.8b06041.

(10) St. Louis, V. L.; Rudd, J. W. M.; Kelly, C. A.; Beaty, K. G.; Flett, R. J.; Roulet, N. T. Production and Loss of Methylmercury and Loss of Total Mercury from Boreal Forest Catchments Containing Different Types of Wetlands. *Environ Sci Technol* **1996**, *30* (9), 2719–2729. https://doi.org/10.1021/es950856h.

(11) Mitchell, C. P. J.; Branfireun, B. A.; Kolka, R. K. Spatial Characteristics of Net Methylmercury Production Hot Spots in Peatlands. *Environ Sci Technol* **2008**, *42* (4), 1010–1016. https://doi.org/10.1021/es0704986.

(12) Gilmour, C. C.; Riedel, G. S.; Ederington, M. C.; Bell, J. T.; Benoit, J. M. Methylmercury Concentrations and Production Rates across a. *Trophic Gradient in the Northern Everglades. Biogeochemistry* **1998**, *40* (2–3), 327–345.

(13) Pollman, C. D. Major Drivers of Mercury Methylation and Cycling in the Everglades: A Synthesis. In *Mercury and the Everglades. A Synthesis and Model for Complex Ecosystem Restoration*; Springer International Publishing: Cham, 2019. https://doi.org/10.1007/978-3-030-32057-7_6.

(14) Orem, W.; Gilmour, C.; Axelrad, D.; Krabbenhoft, D.; Scheidt, D.; Kalla, P.; McCormick, P.; Gabriel, M.; Aiken, G. Sulfur in the South Florida Ecosystem: Distribution, Sources, Biogeochemistry, Impacts, and Management for Restoration. *Crit Rev Environ Sci Technol* **2011**, *41* (SUPPL. 1), 249–288. https://doi.org/10.1080/10643389.2010.531201.

(15) Arndt, S.; Jørgensen, B. B.; LaRowe, D. E.; Middelburg, J. J.; Pancost, R. D.; Regnier, P. Quantifying the Degradation of Organic Matter in Marine Sediments: A Review and Synthesis. *Earth Sci Rev* **2013**, *123*, 53–86. https://doi.org/10.1016/j.earscirev.2013.02.008.

(16) Bae, H. S.; Dierberg, F. E.; Ogram, A. Syntrophs Dominate Sequences Associated with the Mercury Methylation-Related Gene HgcA in the Water Conservation Areas of the Florida Everglades. *Appl Environ Microbiol* **2014**, *80* (20), 6517–6526. https://doi.org/10.1128/AEM.01666-14.

(17) Graham, A. M.; Aiken, G. R.; Gilmour, C. C. Effect of Dissolved Organic Matter Source and Character on Microbial Hg Methylation in Hg-S-DOM Solutions. *Environ Sci Technol* **2013**, *47* (11), 5746–5754. https://doi.org/10.1021/es400414a.

(18) Luek, J. L.; Thompson, K. E.; Larsen, R. K.; Heyes, A.; Gonsior, M. Sulfate Reduction in Sediments Produces High Levels of Chromophoric Dissolved Organic Matter. *Sci Rep* **2017**, *7* (1), 1–8. https://doi.org/10.1038/s41598-017-09223-z.

(19) Haitzer, M.; Aiken, G. R.; Ryan, J. N. Binding of Mercury(II) to Dissolved Organic Matter: The Role of the Mercury-to-DOM Concentration Ratio. *Environ Sci Technol* **2002**, *36* (16), 3564–3570. https://doi.org/10.1021/es025699i.

(20) Gerbig, C. A.; Kim, C. S.; Stegemeier, J. P.; Ryan, J. N.; Aiken, G. R. Formation of Nanocolloidal Metacinnabar in Mercury-DOM-Sulfide Systems. *Environ Sci Technol* **2011**, *45* (21), 9180–9187. https://doi.org/10.1021/es201837h.

(21) Poulin, B. A.; Gerbig, C. A.; Kim, C. S.; Stegemeier, J. P.; Ryan, J. N.; Aiken, G. R. Effects of Sulfide Concentration and Dissolved Organic Matter Characteristics on the Structure of Nanocolloidal Metacinnabar. *Environ Sci Technol* **2017**, *51* (22), 13133–13142. https://doi.org/10.1021/acs.est.7b02687.

(22) Poulin, B. A.; Ryan, J. N.; Nagy, K. L.; Stubbins, A.; Dittmar, T.; Orem, W.; Krabbenhoft, D. P.; Aiken, G. R. Spatial Dependence of Reduced Sulfur in Everglades Dissolved Organic Matter Controlled by Sulfate Enrichment. *Environ Sci Technol* **2017**, *51* (7), 3630–3639. https://doi.org/10.1021/acs.est.6b04142.

(23) Janssen, S. E.; Tate, M. T.; Poulin, B. A.; Krabbenhoft, D. P.; DeWild, J. F.; Ogorek, J. M.; Varonka, M. S.; Orem, W. H.; Kline, J. L. Decadal Trends of Mercury Cycling and Bioaccumulation within Everglades National Park. *Science of the Total Environment* **2022**, *838* (March), 156031. https://doi.org/10.1016/j.scitotenv.2022.156031.

(24) Cleckner, L. B.; Garrison, P. J.; Hurley, J. P.; Olson, M. L.; Krabbenhoft, P. Trophic Transfer of Methyl Mercury in the Northern Florida Everglades Mercury as Global Pollutant. *Biochemistry* **1998**, *40* (2), 347–361.

(25) Mason, R. P.; Reinfelder, J. R.; Morel, F. M. M. Uptake, Toxicity, and Trophic Transfer of Mercury in a Coastal Diatom. *Environ Sci Technol* **1996**, *30* (6), 1835–1845. https://doi.org/10.1021/es950373d.

(26) Xiang, Y.; Liu, G.; Yin, Y.; Cai, Y. Periphyton as an Important Source of Methylmercury in Everglades Water and Food Web. *J Hazard Mater* **2021**, *410* (November 2020), 124551. https://doi.org/10.1016/j.jhazmat.2020.124551.

(27) Moye, H. A.; Miles, C. J.; Phlips, E. J.; Sargent, B.; Merritt, K. K. Kinetics and Uptake Mechanisms for Monomethylmercury between Freshwater Algae and Water. *Environ Sci Technol* **2002**, *36* (16), 3550–3555. https://doi.org/10.1021/es011421z.

(28) Tate, M. T.; Dewild, J. F.; Ogorek, J. M.; Janssen, S. E.; Krabbenhoft, D. P.; Poulin, B. A.; Breitmeyer, S. E.; Aiken, G. R.; Orem, W. H.; Varonka, M. S. Chemical Characterization of Water, Sediments, and Fish from Water Conservation Areas and Canals of the Florida Everglades (USA), 2012 to 2019. *U.S. Geological Survey Data Release* **2023**. https://doi.org/https://doi.org/10.5066/P976EGIX.

(29) Wilson, B. J.; Servais, S.; Mazzei, V.; Kominoski, J. S.; Hu, M.; Davis, S. E.; Gaiser, E.; Sklar, F.; Bauman, L.; Kelly, S.; Madden, C.; Richards, J.; Rudnick, D.; Stachelek, J.; Troxler, T. G. Salinity Pulses Interact with Seasonal Dry-down to Increase Ecosystem Carbon Loss in Marshes of the Florida Everglades. *Ecological Applications* **2018**, *28* (8), 2092–2108. https://doi.org/10.1002/eap.1798.

(30) Chambers, L. G.; Reddy, K. R.; Osborne, T. Z. Short-Term Response of Carbon Cycling to Salinity Pulses in a Freshwater Wetland. *Soil Science Society of America Journal* **2011**, *75* (5), 2000–2007. https://doi.org/10.2136/sssaj2011.0026.

(31) Servais, S.; Kominoski, J. S.; Charles, S. P.; Gaiser, E. E.; Mazzei, V.; Troxler, T. G.; Wilson, B. J. Saltwater Intrusion and Soil Carbon Loss: Testing Effects of Salinity and Phosphorus Loading on Microbial Functions in Experimental Freshwater Wetlands. *Geoderma* **2019**, *337* (December 2017), 1291–1300. https://doi.org/10.1016/j.geoderma.2018.11.013.

(32) Gaiser, E.; Childers, D. Water Quality Data (Grab Samples) from the Shark River Slough, Everglades National Park (FCE LTER). *Environmental Data Initiative* **2022**. https://doi.org/https://doi.org/10.6073/pasta/4c6a5c2382bf376c8872560fc32be14e.

(33) Park, J.; Stabenau, E.; Redwine, J.; Kotun, K. South Florida's Encroachment of the Sea and Environmental Transformation over the 21st Century. *J Mar Sci Eng* **2017**, *5* (3), 1–26. https://doi.org/10.3390/jmse5030031.

(34) Castaneda, E.; Rivera-Monroy, V. H. Abiotic Monitoring of Physical Characteristics in Porewaters and Surface Waters of Mangrove Forests from the Shark River Slough and Taylor Slough. *Everglades National Park (FCE LTER), South Florida, USA* **2022**. https://doi.org/https://doi.org/10.6073/pasta/285bc87dc9418e5f0579f72d1e00b6d9.

(35) Aiken, G. R.; McKnight, D. M.; Thorn, K. A.; Thurman, E. M. Isolation of Hydrophilic Organic Acids from Water Using Nonionic Macroporous Resins. *Org Geochem* **1992**, *18* (4), 567–573. https://doi.org/10.1016/0146-6380(92)90119-I.

(36) Pucher, M.; Wünsch, U.; Weigelhofer, G.; Murphy, K.; Hein, T.; Graeber, D. StaRdom: Versatile Software for Analyzing Spectroscopic Data of Dissolved Organic Matter in R. *Water (Basel)* **2019**, *11* (11), 2366. https://doi.org/10.3390/w11112366.

(37) Helms, J. R.; Stubbins, A.; Ritchie, J. D.; Minor, E. C.; Kieber, D. J.; Mopper, K. Absorption Spectral Slopes and Slope Ratios as Indicators of Molecular Weight, Source, and Photobleaching of Chromophoric Dissolved Organic Matter. *Limnol Oceanogr* **2008**, *53* (3), 955–969. https://doi.org/10.4319/lo.2008.53.3.0955.

(38) Weishaar, J. L.; Aiken, G. R.; Bergamaschi, B. A.; Fram, M. S.; Fujii, R.; Mopper, K. Evaluation of Specific Ultraviolet Absorbance as an Indicator of the Chemical Composition and Reactivity of Dissolved Organic Carbon. *Environ Sci Technol* **2003**, *37* (20), 4702–4708. https://doi.org/10.1021/es030360x.

(39) Schecher, W. D.; McAvoy, D. C. MINEQL+: A Software Environment for Chemical Equilibrium Modeling. *Comput Environ Urban Syst* **1992**, *16* (1), 65–76. https://doi.org/10.1016/0198-9715(92)90053-T.

(40) Sleighter, R. L.; Chin, Y.-P.; Arnold, W. A.; Hatcher, P. G.; McCabe, A. J.; McAdams, B. C.; Wallace, G. C. Evidence of Incorporation of Abiotic S and N into Prairie Wetland Dissolved Organic Matter. *Environ Sci Technol Lett* **2014**, *1* (9), 345–350. https://doi.org/10.1021/ez500229b.

(41) Chambers, L. G.; Davis, S. E.; Troxler, T.; Boyer, J. N.; Downey-Wall, A.; Scinto, L. J. Biogeochemical Effects of Simulated Sea Level Rise on Carbon Loss in an Everglades Mangrove Peat Soil. *Hydrobiologia* **2014**, *726* (1), 195–211. https://doi.org/10.1007/s10750-013-1764-6.

(42) Ardón, M.; Helton, A. M.; Bernhardt, E. S. Drought and Saltwater Incursion Synergistically Reduce Dissolved Organic Carbon Export from Coastal Freshwater Wetlands. *Biogeochemistry* **2016**, *127* (2–3), 411–426. https://doi.org/10.1007/s10533-016-0189-5.

(43) Kreuzburg, M.; Rezanezhad, F.; Milojevic, T.; Voss, M.; Gosch, L.; Liebner, S.; Van Cappellen, P.; Rehder, G. Carbon Release and Transformation from Coastal Peat Deposits Controlled by Submarine Groundwater Discharge: A Column Experiment Study. *Limnol Oceanogr* **2020**, *65* (5), 1116–1135. https://doi.org/10.1002/lno.11438.

(44) Liu, H.; Lennartz, B. Short Term Effects of Salinization on Compound Release from Drained and Restored Coastalwetlands. *Water (Switzerland)* **2019**, *11* (8). https://doi.org/10.3390/w11081549.

(45) Poulin, B. A.; Aiken, G. R.; Nagy, K. L.; Manceau, A.; Krabbenhoft, D. P.; Ryan, J. N. Mercury Transformation and Release Differs with Depth and Time in a Contaminated Riparian Soil during Simulated Flooding. *Geochim Cosmochim Acta* **2016**, *176*, 118–138. https://doi.org/10.1016/j.gca.2015.12.024.

(46) Weber, F. A.; Voegelin, A.; Kretzschmar, R. Multi-Metal Contaminant Dynamics in Temporarily Flooded Soil under Sulfate Limitation. *Geochim Cosmochim Acta* **2009**, *73* (19), 5513–5527. https://doi.org/10.1016/j.gca.2009.06.011.

(47) Skyllberg, U.; Drott, A. Competition between Disordered Iron Sulfide and Natural Organic Matter Associated Thiols for Mercury(II) - An EXAFS Study. *Environ Sci Technol* **2010**, *44* (4), 1254–1259. https://doi.org/10.1021/es902091w.

(48) Gong, Y.; Yin, J.; Zhang, T.; Yin, W.; Sun, L.; Liang, Q.; Wang, Q. Ferrous Sulfide Nanoparticles Control Mercury Speciation and Bioavailability to Methylating Bacteria in Contaminated Groundwater: Impacts of Mercury Species. *Chemical Engineering Journal* **2023**, *455* (November 2022), 140612. https://doi.org/10.1016/j.cej.2022.140612.

(49) Ulrich, P. D.; Sedlak, D. L. Impact of Iron Amendment on Net Methylmercury Export from Tidal Wetland Microcosms. *Environ Sci Technol* **2010**, *44* (19), 7659–7665. https://doi.org/10.1021/es1018256.

(50) Gilmour, C.; Krabbenhoft, D.; Orem, W.; Aiken, G. Appendix 2B-1: Influence of Drying and Rewetting on Hg and S Cycling in Everglades and STA Soils, AQUATIC CYCLING OF MERCURY IN THE EVERGLADES (ACME) GROUP PRELIMINARY DRY/REWET EXPERIMENTS (2/02-1/03). *Everglades Consolidated Report* **2004**.

(51) Graham, A. M.; Cameron-Burr, K. T.; Hajic, H. A.; Lee, C.; Msekela, D.; Gilmour, C. C. Sulfurization of Dissolved Organic Matter Increases Hg-Sulfide-Dissolved Organic Matter Bioavailability to a Hg-Methylating Bacterium. *Environ Sci Technol* **2017**, *51* (16), 9080–9088. https://doi.org/10.1021/acs.est.7b02781.

(52) Orem, W.; Fitz, H. C.; Krabbenhoft, D.; Tate, M.; Gilmour, C.; Shafer, M. Modeling Sulfate Transport and Distribution and Methylmercury Production Associated with Aquifer Storage and Recovery Implementation in the Everglades Protection Area. *Sustainability of Water Quality and Ecology* **2014**, *3*, 33–46. https://doi.org/10.1016/j.swaqe.2014.11.004.

(53) Gilmour, C. C.; Podar, M.; Bullock, A. L.; Graham, A. M.; Brown, S. D.; Somenahally, A. C.; Johs, A.; Hurt, R. A.; Bailey, K. L.; Elias, D. A. Mercury Methylation by Novel Microorganisms from New Environments. *Environ Sci Technol* **2013**, *47* (20), 11810–11820. https://doi.org/10.1021/es403075t.

(54) Bergamaschi, B. A.; Krabbenhoft, D. P.; Aiken, G. R.; Patino, E.; Rumbold, D. G.; Orem, W. H. Tidally Driven Export of Dissolved Organic Carbon, Total Mercury, and Methylmercury from a Mangrove-Dominated Estuary. *Environ Sci Technol* **2012**, *46* (3), 1371–1378. https://doi.org/10.1021/es2029137.

(55) Drexel, R. T.; Haitzer, M.; Ryan, J. N.; Aiken, G. R.; Nagy, K. L. Mercury(II) Sorption to Two Florida Everglades Peats: Evidence for Strong and Weak Binding and Competition by Dissolved Organic Matter Released from the Peat. *Environ Sci Technol* **2002**, *36* (19), 4058–4064. https://doi.org/10.1021/es0114005.

(56) Hintelmann, H.; Falter, R.; Ilgen, G.; Evans, R. D. Determination of Artifactual Formation of Monomethylmercury (CH 3 Hg +) in Environmental Samples Using Stable Hg 2+ Isotopes with ICP-MS Detection: Calculation of Contents Applying Species Specific Isotope Addition. *Fresenius J Anal Chem* **1997**, *358* (3), 363–370. https://doi.org/10.1007/s002160050431.

(57) Amirbahman, A.; Reid, A. L.; Haines, T. A.; Kahl, J. S.; Arnold, C. Association of Methylmercury with Dissolved Humic Acids. *Environ Sci Technol* **2002**, *36* (4), 690–695. https://doi.org/10.1021/es011044q.

(58) Qian, J.; Skyllberg, U.; Frech, W.; Bleam, W. F.; Bloom, P. R.; Petit, P. E. Bonding of Methyl Mercury to Reduced Sulfur Groups in Soil and Stream Organic Matter as Determined by X-Ray Absorption Spectroscopy and Binding Affinity Studies. *Geochim Cosmochim Acta* **2002**, *66* (22), 3873–3885. https://doi.org/10.1016/S0016-7037(02)00974-2.

(59) Zhao, X.; Rivera-Monroy, V. H.; Wang, H.; Xue, Z. G.; Tsai, C. F.; Willson, C. S.; Castañeda-Moya, E.; Twilley, R. R. Modeling Soil Porewater Salinity in Mangrove Forests (Everglades, Florida, USA) Impacted by Hydrological Restoration and a Warming Climate. *Ecol Modell* **2020**, *436* (September), 109292. https://doi.org/10.1016/j.ecolmodel.2020.109292.

(60) Rumbold, D. G.; Evans, D. W.; Niemczyk, S.; Fink, L. E.; Laine, K. A.; Howard, N.; Krabbenhoft, D. P.; Zucker, M. Source Identification of Florida Bay's Methylmercury Problem: Mainland Runoff Versus Atmospheric Deposition and In Situ Production. *Estuaries and Coasts* **2011**, *34* (3), 494–513. https://doi.org/10.1007/s12237-010-9290-5.

(61) Mitchell, C. P. J.; Gilmour, C. C. Methylmercury Production in a Chesapeake Bay Salt Marsh. *J Geophys Res Biogeosci* **2008**, *113* (G2), n/a-n/a. https://doi.org/10.1029/2008jg000765.

(62) Mitchell, C. P. J.; Jordan, T. E.; Heyes, A.; Gilmour, C. C. Tidal Exchange of Total Mercury and Methylmercury between a Salt Marsh and a Chesapeake Bay Sub-Estuary. *Biogeochemistry* **2012**, *111* (1–3), 583–600. https://doi.org/10.1007/s10533-011-9691-y.

(63) Lacerda, L. D.; Silva, L. F. F.; Marins, R. V.; Mounier, S.; Paraquetti, H. H. M.; Benaim, J. Dissolved Mercury Concentrations and Reactivity in Mangrove Waters from the Itacurussa Experimental Forest, Sepetiba Bay, SE Brazil. *Wetl Ecol Manag* **2001**, *9* (4), 323–331. https://doi.org/10.1023/A:1011868803439.

(64) Guédron, S.; Huguet, L.; Vignati, D. A. L.; Liu, B.; Gimbert, F.; Ferrari, B. J. D.; Zonta, R.; Dominik, J. Tidal Cycling of Mercury and Methylmercury between Sediments and Water Column in the Venice Lagoon (Italy). *Mar Chem* **2012**, *130–131*, 1–11. https://doi.org/10.1016/j.marchem.2011.12.003.

(65) Chambers, L. G.; Guevara, R.; Boyer, J. N.; Troxler, T. G.; Davis, S. E. Effects of Salinity and Inundation on Microbial Community Structure and Function in a Mangrove Peat Soil. *Wetlands* **2016**, *36* (2), 361–371. https://doi.org/10.1007/s13157-016-0745-8.

(66) Chiang, G.; Kidd, K. A.; Díaz-Jaramillo, M.; Espejo, W.; Bahamonde, P.; O'Driscoll, N. J.; Munkittrick, K. R. Methylmercury Biomagnification in Coastal Aquatic Food Webs from Western Patagonia and Western Antarctic Peninsula. *Chemosphere* **2021**, *262*, 128360. https://doi.org/10.1016/j.chemosphere.2020.128360.

(67) Damseaux, F.; Kiszka, J. J.; Heithaus, M. R.; Scholl, G.; Eppe, G.; Thomé, J. P.; Lewis, J.; Hao, W.; Fontaine, M. C.; Das, K. Spatial Variation in the Accumulation of POPs and Mercury in Bottlenose Dolphins of the Lower Florida Keys and the Coastal Everglades (South Florida). *Environmental Pollution* **2017**, *220*, 577–587. https://doi.org/10.1016/j.envpol.2016.10.005.

Appendix

Table A-1. MINEQL+ Modelling Parameters and Thermodynamic Constants

Component Groups	
Component	**Concentration (M)**
Fe^{2+}	1e-18
Fe^{3+}	2e-5
HS^{-}	1e-5
H^{+}	1e-18

H_2O	1e-18
e^-	1e-18

Aqueous Conditions

Parameter	Value
pH	6.30
Temperature	25˚C

Titration Conditions

Parameter	Start	End	No. of Points
Ionic Strength (M)	0	0.12	100

Thermo Summary

Reaction	Log K
$H_2O = OH^- + H^+$	-13.997[1]
$H_2O + Fe^{2+} = FeOH^+ + H^+$	-9.397[2]
$2H_2O + Fe^{2+} = Fe(OH)_2 + 2H^+$	-20.494[2]
$3H_2O + Fe^{2+} = Fe(OH)_3^- + 3H^+$	-28.991[2]
$4H_2O + 3Fe^{3+} = Fe_3(OH)_4^{5+} + 4H^+$	-6.288[2]
$4H_2O + Fe^{3+} = Fe(OH)_4^- + 4H^+$	-21.588[2]
$3H_2O + Fe^{3+} = Fe(OH)_3 + 3H^+$	-12.560[3]
$2H_2O + 2Fe^{3+} = Fe_2(OH)_2^{4+} + 2H^+$	-2.854[2]
$2H_2O + Fe^{3+} = Fe(OH)_2^+ + 2H^+$	-4.594[2]
$H_2O + Fe^{3+} = FeOH^{2+} + H^+$	9.993[2]
$HS^- = S^{2-} + H^+$	-17.300[4]
$H^+ + HS^- = H_2S$	7.020[2]
$Fe^{2+} + 2HS^- = Fe(H_2)_2$	8.950[5]
$Fe^{2+} + 3HS^- = Fe(H_3)_3^-$	10.987[5]
$e^- + Fe^{3+} = Fe^{2+}$	13.032[6]

Potential Precipitates

Reaction	Solid Name	Log K
$H_2O + 0.95Fe^{2+} = Fe_{0.95}O + 2H^+$	Wustite	-11.688[7]
$2H_2O + Fe^{2+} = Fe(OH)_2 + 2H^+$	$Fe(OH)_2$	-13.564[1]
$4H_2O + Fe^{2+} + 2Fe^{3+} = FeFe_2O_4 + 8H^+$	Magnetite	-3.403[7]
$8H_2O + Fe^{2+} + 2Fe^{3+} = FeFe_2(OH)_8 + 8H^+$	$Fe_3(OH)_8$	-20.222[5]
$2H_2O + Fe^{3+} = FeO{-}OH + 3H^+$	Goethite	-0.491[1]
$2H_2O + Fe^{3+} = FeO{-}OH + 3H^+$	Lepidocrocite	-1.371[5]
$3H_2O + 2Fe^{3+} = Fe_2O_3 + 6H^+$	Hematite	1.418[1]
$3H_2O + Fe^{3+} = Fe(OH)_3 + 3H^+$	Ferrihydrite	-3.191[1]
$3H_2O + 2Fe^{3+} = Fe_2O_3 + 6H^+$	Maghemite	-6.386[5]
$Fe^{2+} + 2Fe^{3+} + 4HS^- = FeFe_2S_4 + 4H^+$	Greigite	45.035[5]
$Fe^{2+} + HS^- = FeS + H^+$	Mackinawite	3.600[8]
$Fe^{2+} + HS^- = FeS + H^+$	FeS (ppt)	2.950[8]

1. Critical Stability Constants of Metal Complexes Database (1997). NIST StandardReference Database 46, ver 4.0, National Institute of Standards and Technology.

2. Critical Stability Constants of Metal Complexes Database (1996). NIST Standard Reference Database 46, ver 3.0, National Institute of Standards and Technology.
3. Nordstrom, D.K., L.N. Plummer, D. Langmuir, E. Busenberg, H. May, B.L. Jones, and D.L. Parkhurst (1990). Revised chemical equilibrium data for major water-mineral reactions and their limitations. In: D.C. Melchior and R.L. Bassett, (eds), Chemical Modeling in Aqueous Systems II, American Chemical Society Symposium Series 416, 398
4. Licht, S. and J. Manassen (1987). The Second Dissociation Constant of H2S J. Electrochem. Soc.,134(4), 918-921.
5. Allison, J.D., D.S. Brown, and K.J. Novo-Gradac (1991). MINTEQA2/PRODEFA2, A Geochemical Assessment Model for Environmental Systems: Version 3.0 User's Manual, United States Environmental Protection Agency, Office of Research and Development, Washington, DC, EPA/600/3-91/021.
6. International Union of Pure and Applied Chemistry (IUPAC) (1985). Standard Potentials in Aqueous Solution, Marcel Dekker, Inc., New York..
7. NIST JANAF Thermochemical Tables (1985). NIST Standard Reference Database 13, ver 1.0, National Institute of Standards and Technology.
8. Davison, W. (1991). The solubility of iron sulphides in synthetic and natural waters at ambient temperature, Aquatic Sciences,53, 309.